Published in final edited form as:

Cell Rep. 2023 June 27; 42(6): 112580. doi:10.1016/j.celrep.2023.112580.

Distinct bidirectional regulation of LFA1 and α4β7 by Rap1 and integrin adaptors in T cells under shear flow

Yuji Kamioka[1], **Yoshihiro Ueda**[1], **Naoyuki Kondo**[1], **Keizo Tokuhiro**[2], **Yoshiki Ikeda**[1], **Wolfgang Bergmeier**[3], **Tatsuo Kinashi**[1,4,*]

[1]Department of Molecular Genetics, Institute of Biomedical Science, Kansai Medical University, Osaka, Japan

[2]Department of Genome Editing, Institute of Biomedical Science, Kansai Medical University, Osaka, Japan

[3]Department of Biochemistry and Biophysics, Blood Research Center, University of North Carolina at Chapel Hill, Chapel Hill, NC, USA

[4]Lead contact

SUMMARY

Bidirectional control of integrin activation plays crucial roles in cell adhesive behaviors, but how integrins are specifically regulated by inside-out and outside-in signaling has not been fully understood. Here, we report distinct bidirectional regulation of major lymphocyte homing receptors LFA1 and α4β7 in primary T cells. A small increase of Rap1 activation in L-selectin-mediated tether/rolling was boosted by the outside-in signaling from ICAM1-interacting LFA1 through subsecond, simultaneous activation of Rap1 GTPase and talin1, but not kindlin-3, resulting in increased capture and slowing. In contrast, none of them were required for tether/rolling by α4β7 on MAdCAM1. High Rap1 activation with chemokines or the loss of Rap1-inactivating proteins Rasa3 and Sipa1 increased talin1/kindlin-3-dependent arrest with high-affinity binding of LFA1 to membrane-anchored ICAM1. However, despite increased affinity of α4β7, activated Rap1 severely suppressed adhesion on MAdCAM1 under shear flow, indicating the critical importance of a sequential outside-in/inside-out signaling for α4β7.

Graphical abstract

*Correspondence: kinashi@hirakata.kmu.ac.jp.

AUTHOR CONTRIBUTIONS

Y.K. performed experiments, analyzed data, and wrote the manuscript. Y.U. and N.K. performed experiments and analyzed data. K.T. and Y.K. created genetically modified mice. W.B. offered genetically modified mice and critical reading and suggestions for the manuscript. Y.I. provided useful advice and discussion. T.K. supervised the research and wrote the manuscript.

SUPPLEMENTAL INFORMATION

Supplemental information can be found online at https://doi.org/10.1016/j.celrep.2023.112580.

DECLARATION OF INTERESTS

The authors declare no competing interests.

INCLUSION AND DIVERSITY

We support inclusive, diverse, and equitable conduct of research.

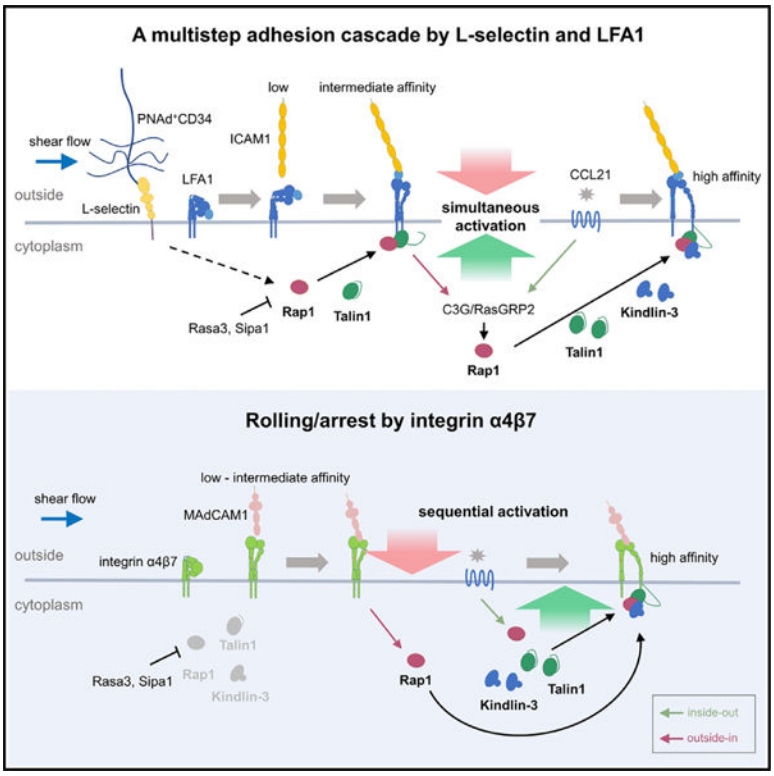

In brief

Kamioka et al. reveal that Rap1 and integrin adaptors talin1 and kindlin-3 differently regulate two major homing integrins, LFA1 and α4β7, in T cells, resulting in distinct impacts by Rap1 on affinity of LFA1 and α4β7, generating promotion or inhibition of adhesion of T cells under flow conditions.

INTRODUCTION

Lymphocyte entry into peripheral lymph nodes (LNs) occurs at specialized post-capillary venules called high endothelial venules (HEVs). In the original multistep model, lymphocyte L-selectin interacts with sulfated glycans, peripheral node addressin (PNAd) mediates rolling on the HEV in peripheral LNs, and chemokine-triggered activation of LFA1 (αLβ2) and α4 integrins mediates arrest adhesion and subsequent transmigration.[1–3] Although it is generally selectins that mediate rolling, α4 integrins, especially α4β7, can mediate both the rolling and arrest of lymphocytes.[1,2] The α4β7 integrin expressed on a subset of lymphocytes is a homing receptor for mucosal lymphoid tissues, mediated through binding to mucosal addressin cell adhesion molecule 1 (MAdCAM1).[3] LFA1 and ICAM1 have an additional role in supporting rolling adhesion of neutrophils by E/P-selectins[4] or directly mediating rolling in cell lines.[5–7] It is generally thought that integrins such as LFA1 are kept in low-affinity states with bent/closed conformations at baseline, extended/closed conformers (intermediate affinity) to support or mediate rolling, and open/extended conformers (high affinity) to mediate arrest.[4,8–10]

Recent advancement in the understanding of structural and molecular findings that regulate integrin activation by ligands and intracellular signaling to integrin adaptor proteins talin1 and kindlin-3 have revisited the key issue regarding how integrin occupancy with adaptor proteins and ligand binding cooperatively regulate dynamic adhesion responses of immune cells in diverse microenvironments.[11–14] It is widely thought that bidirectional integrin activation through intracellular signaling triggered by chemokines and T cell receptor (TCR) (inside-out signal) and ligand binding (outside-in signal) shift the bent conformations to extended and open conformations, leading to arrest and firm adhesion.[4,14–17] Integrin adaptors play crucial roles in integrin adhesive functions by binding to distinct sites of the cytoplasmic β subunit regions of integrins.[18] Lefort et al. demonstrated that kindlin-3 is involved in the arrest step of neutrophils, while talin1 is required for both slow rolling by extended LFA1 and arrest by open/extended LFA1.[8] We previously reported a novel function of kindlin-3 in the unclasping of intersubunit associations of LFA1, which promotes the high-affinity binding of talin1 to the β2 tail and adhesion to ICAM1.[19]

The small GTPase Rap1 is the master regulator of inside-out signaling by chemokines and antigen receptors.[16,20] Interactions of PSGL-1 on neutrophils with E/P-selectin is another pathway to activate Rap1, which induces slow rolling through extended/closed LFA1.[14,21] The highly homologous Rap1 isoforms, Rap1a and Rap1b, are expressed in hematopoietic cells with greater amounts of Rap1b in T cells.[22] Knockout (KO) of both *Rap1a* and *Rap1b* genes in conventional T cells severely impaired chemokine- and TCR-induced integrin-mediated adhesion and immunological synapse formation,[22–25] as well as regulatory T cell adhesion by LFA1, α4β1, and α4β7.[26] Rap1, like other small GTPases, cycles between a GDP-bound inactive state and GTP-bound active state regulated by activating guanine exchange factors (GEFs) and inactivating GTPase-activating proteins (GAPs). The Rap1GEFs (RasGRP2 [CalDAG-GEFI][27] and C3G [RapGEFI][28,29]) and RapGAPs (Rasa3[14,30] and Sipa1[31]) regulate Rap1 activation and cellular functions including integrins in leukocytes and platelets. Membrane recruitment of talin1 is mediated by Rap1 directly,[32] or by PIP2 produced by PIP5KIγ[33] or through Rap1-interacting adapter molecule (RIAM).[34] The ablation of PIP2-producing PIP5KI had modest impacts on the talin-mediated adhesion,[35] and double KO of PIP5KI and Rap1 has shown that PIP5KI and Rap1 cooperatively regulate the neutrophil slow rolling and arrest.[36] Membrane recruitment of kindlin-3 also appears to involve multiple pathways via Rap1[19,22] as well as via the PIP3-binding pleckstrin homology (PH) domain of kindlin-3,[37] and it occurs before induction of open-extended/high-affinity LFA1 in the transition from neutrophil rolling to arrest.[38] The complexity of regulations of Rap1 and integrin adaptors makes it difficult to clarify how Rap1 and integrin adaptors are involved in lymphocyte rolling and arrest in a coordinated way.

In this study, we show the distinct roles of Rap1 and integrin adaptors in homing to peripheral LN and in the regulation of rolling and arrest by LFA1 and α4β7. These findings reveal integrin-specific properties of bidirectional regulation in lymphocyte adhesion cascades.

RESULTS

Relative contributions of integrin adaptors and Rap1 in lymphocyte homing to peripheral LN

To investigate the functions of Rap1 and the integrin adaptors talin1 and kindlin-3 in lymphocyte rolling and arrest, we first compared lymphocyte trafficking to secondary LNs using T cells from mutant mice bearing a T cell-specific deletion of kindlin-3 (Knd3-KO), talin1 (Tln-KO), or Rap1a/Rap1b (Rap1-KO). Compensatory upregulation of kindlin-1 and kindlin-2 in Knd3-KO T cells was not detected with specific antibodies against kindlin-1 and kindlin-2 (Figures S1A and S1B) or talin2 in Tln-KO T cells with an anti-Tln1/2 antibody, respectively (Figure S5C, supplemental methods). We isolated and labeled T cells from the spleen of wild-type (WT) and mutant mice for short homing assays. One hour after being injected intravenously into WT mice, the number of transferred T cells relative to WT was measured in LNs and the spleen (Figures 1A and S1C). T cells from Tln-KO and Rap1-KO mice were severely impaired for homing to surface LNs, mesenteric LNs, and Peyer's patches with efficiencies of less than 5%–10% compared with WT controls, whereas those of Knd3-KO T cells achieved 40%–50% in surface and mesenteric LNs and 25% in Peyer's patches. The decreased impact of kindlin-3 deficiency in T cell homing is consistent with the relatively abundant T cell numbers in the peripheral LNs of Knd3-KO mice compared with those of Tln-KO and Rap1-KO mice (Figure S1D). The spleen homing of mutant T cells appeared to be normal; however, histological examination revealed inefficient entry of all mutant T cells into T cell zones of the white pulp with a decrease of 70%–80% (Figures S1E and S1F). This result is consistent with the previous report showing integrin-dependent migration of T cells along periarteriolar stromal cells from the red to the white pulp.[39] Thus, the absence of integrin adaptors and Rap1 resulted in impaired homing to peripheral LN and T cell zones of the spleen. The numbers of adhesion molecules (L-selectin, LFA1, and $\alpha 4\beta 7$) were basically comparable among the mutant mice (Figure S1G).

Previous studies have reported reduced adhesion of Knd3-KO T cells to HEVs in peripheral LNs.[40] However, relative contributions of Rap1, talin1, and kindlin-3 in attachment to HEVs have remained unclear. HEVs are located at the venular branching orders III–V, according to venular orders I–V from the large collecting venules to the small post-capillary ones.[41] When transferred into mice, WT T cells adhered to HEVs at branching orders III–V. Consistent with their defective homing, both Tln-KO and Rap1-KO T cells failed to attach to MECA-79$^+$ HEVs (Figure 1B). By contrast, Knd3-KO T cells adhered to HEVs mostly at branching order III and to a lesser degree at orders IV and V, compared with WT T cells (Figures 1B, 1C, andS1H). Treatment with anti-LFA1 almost completely inhibited the attachment of Knd3-KO T cells to HEVs (Figure 1D). This result suggests that HEVs with larger diameters, hence low shear stress, allow Knd3-KO T cells to attach via LFA1. Detachment assays showed that all mutant T cells failed to adhere at low densities of ICAM1 (180 sites/μm^2) even with low shear stress (Figure 1E). However, Knd3-KO T cells partially adhered to high-density ICAM1 of 1,000 sites/μm2 at a low shear stress of 2 dyn/cm^2, but not high shear stress (5 dyn/cm^2) (Figure 1F). These results are in line with earlier studies reporting partial impacts of kindlin-3 on effector T cell adhesion to high amounts of ICAM1 of inflamed endothelium[42,43] and indicate that the absence of kindlin-3 impaired

affinity modulation of LFA1 for binding to low-density ICAM1 but maintained adhesiveness to high-density ICAM1 through multivalent binding.

Differential requirements of Rap1, talin1, and kindlin-3 for rolling and arrest by LFA1 and α4β7

Since it was difficult to quantitatively examine the roles of Rap1, talin1, and kindlin-3 in the initial rolling and arrest in lymphocyte homing, we reconstituted lymphocyte multistep adhesion cascades *in vitro* using a parallel-plate flow chamber coated with PNAd$^+$CD34 and/or ICAM1 (Figures 2A and S2A; Video S1). Recombinant CD34-Fc decorated with 6-sulfo sialyl Lewis X were purified from culture supernatants of LS12 cells expressing HEV-specific enzymes for fucosylation and sulfation,[44] and expression of PNAd recognized by MECA-79 was confirmed. PNAd$^+$CD34-Fc supported L-selectin-dependent tether and rolling, resulting in cell accumulation in the ligand-coated area (Figures 2A, 2B, and S2B) (see STAR Methods for details). This was a shear-dependent process as reported previously[45] with a peak at 3–4 dyn/cm^2 under our experimental conditions (Figure S2C). Average rolling velocities of T cells were approximately 30–70 μm/s, which was inversely proportional to the site densities of PNAd$^+$CD34 (Figure 2C). ICAM1 alone did not support rolling adhesion (Figure S2D). Rolling and firm adhesion of T cells was induced when co-immobilized with CCL21, ICAM1 (100 sites/μm2), and PNAd$^+$CD34 (120 sites/μm2) (Figures 2D and S2E; Videos S2 and S3). PNAd$^+$CD34 and ICAM1 in the absence of CCL21 induced rolling but not arrest, indicating a requisite involvement of chemokines in the transition of L-selectin-dependent rolling to arrest by LFA1 and ICAM1. The firm adhesion was abolished in T cells deficient in kindlin-3, talin1, or Rap1 (Figure 2D). Notably, we found that, in the absence of chemokines, ICAM1 augmented capture events (tether/rolling) and reduced rolling velocities of T cells (Figures 2E and S2F). Because the tether/rolling-supportive effects of ICAM1 did not occur with αL-deficient (αL-KO) T cells (Figure 2F), interactions of LFA1 and ICAM1 can support L-selectin-mediated tether/rolling events. Importantly, the tether/rolling-supportive effect by LFA1 was not observed in Tln-KO and Rap1-KO T cells, while Knd3-KO T cells were relatively unaffected (Figure 2G). These results indicated that LFA1/ICAM1 interactions supported tether/rolling by L-selectin in a manner dependent on talin1 and Rap1.

We similarly examined the adhesive interactions of α4β7 with MAdCAM1 in flow conditions. As reported previously,[46] fractions of naive T cells from the spleen and LNs expressed α4β7 and exhibited the mixture of tether, rolling, and arrest on MAdCAM1 without chemokines under shear stress (Figures S2G and S2H; Video S4). This phenotype was in sharp contrast with ICAM1, which rarely supported T cell rolling in flow conditions. Notably, kindlin-3, talin1, or Rap1 deficiency increased the tether/rolling fractions of T cells on MAdCAM1, while the transition from rolling to arrest was impaired in talin1- and Rap1-deficient T cells, and modestly affected in kindlin3-deficient T cells (Figures 2H, S2I, and S2J) with a greater decrease of arrest by CCL21 (Figure S2K). Thus, the unique property of α4β7 supporting tether/rolling of T cells was distinct from LFA1 and did not require Rap1 and integrin adaptor proteins.

Activation of Rap1 via outside-in signaling by LFA1 supports rolling by L-selectin

The above result suggests that Rap1 is activated in T cell rolling on PNAd$^+$CD34 and ICAM1. To measure the Rap1 activation in this process, we introduced a Rap affinity probe (GFP-RalGDS-RBD) into cultured T cells via a lentivirus and measured changes in fluorescence intensities.[19,22,25] We found that intensities of the Rap1 affinity probe increased during rolling on PNAd$^+$CD34 and ICAM1 (Figures 3A–3E; Video S5). With PNAd$^+$CD34 alone, or αL-KO T cells on PNAd$^+$CD34 and ICAM1, rolling T cells exhibited approximately half the intensities of the probe compared with those in normal T cells on PNAd$^+$CD34 and ICAM1 (Figures 3F, 3G, S3A, and S3B). T cells expressing a Venus fluorescent protein (control) did not show a significant increase when they were rolled on PNAd$^+$CD34 and ICAM1 (Figures S3C and S3D). Together, these results suggest that L-selectin and LFA1 activates Rap1 when interacting with their respective ligands under flow conditions.

To gain insight into the mechanism of Rap1 activation in rolling and arrest, we examined Rap1 guanine-nucleotide exchange factors, C3G and RasGRP2, which are involved in integrin activation including platelets and lymphocytes[27–29,47] (Figures S4A–S4D). Using T cells deficient in C3G and RasGRP2, we first examined Rap1 activation by chemokines with pull-down assays. Rap1 activation in WT T cells occurred rapidly within 5 s after stimulation with CCL21. The absence of both proteins reduced Rap1 activation by 90% relative to WT (Figure S4E). In agreement with the amount of Rap1 activation, C3G/RasGRP2 double-deficient T cells (C3G/RasGRP2-KO) exhibited impaired shear-resistant adhesion to ICAM1 more severely than single-mutant T cells (Figure S4F). The absence of C3G and RasGRP2 did not affect tether/rolling events on PNAd$^+$CD34 (Figure S4G). In contrast, the capture frequency of C3G/RasGRP2-KO T cells on PNAd$^+$CD34 and ICAM1 was reduced to 30% relative to WT (Figure S4H), and Rap1 activation in C3G/RasGRP2-KO T cells was almost abolished (Figures 3H and 3I). These findings indicate that both C3G and RasGRP2 are responsible for Rap1 activation to strengthen tether/rolling as well as for chemokine-triggered firm adhesion of T cells.

Next, we investigated an involvement of talin1 in Rap1 activation during rolling on PNAd$^+$CD34 and ICAM1 in the absence of chemokines. Tln-KO T cells did not exhibit Rap1 activation (Figures 3J and 3K), as observed in C3G/RasGRP2-KO T cells. This result indicate that Rap1 activation require talin1 as well as ICAM1, supporting the notion that bidirectional regulation of LFA1 by talin1 and ICAM1 activate Rap1 under flow condition. To clarify when talin1 is recruited in rolling, we used T cells derived from HaloTag-talin1 (HT-Tln1) knockin mice (Figures S5A–S5D) to visualize accumulation of talin1 in rolling. Expression of HT-Tln1 did not affect that of L-selectin and LFA1(Figures S5E and S5F), and also had little impact on adhesion (Figure S5G). Intensity of HT-Tln1 increased concomitant with deceleration of velocities on PNAd$^+$CD34 and ICAM1(Figures 3L, 3M, and S5H–S5J; Video S6). Rolling on PNAd$^+$CD34 alone also induced significantly increased intensity of HT-Tln1 (Figures 3N–3O). Thus, talin1 accumulation and Rap1 activation occurred synchronously, suggesting that the interaction of LFA1 with ICAM1 and talin1 occurred almost simultaneously under shear flow, resulting in instantaneous Rap1 activation.

High-affinity ICAM1 binding in T cells deficient for RapGAPs

To get further insight into the importance of Rap1 activation in adhesion cascades by LFA1 and α4β7, we examined the impact of inactivation of two GAPs for Rap1, Rasa3 and Sipa1. While the single loss of Rasa3 but not Sipa1 augmented basal adhesion (Y.U. et al., unpublished data), double-deficient T cells (Rasa3/Sipa1-KO) showed strong shear-resistant attachment to ICAM1 without chemokine stimulation (Figure 4A). The increased adhesion of Rasa3/Sipa1-KO T cells was almost abolished by the further loss of Rap1 (*Cd4-cre; Rasa3*$^{f/f}$; *Sipa1*$^{-/-}$; *Rap1a*$^{f/f}$; *Rap1b*$^{f/f}$) or talin1 (*Cd4-cre; Rasa3*$^{f/f}$; *Sipa1*$^{-/-}$; *Talin1*$^{f/f}$) (Figure 4A), indicating that the increased adhesion depended on Rap1 and talin1. While LFA1 and α4β7 are normally expressed in Rasa3/Sipa1-KO T cells, L-selectin was increased by approximately 20% compared with that of the control (Figure S6A). Accordingly, the capture frequencies of Rasa3/Sipa1-KO T cells on PNAd^{+}CD34 were increased by approximately 20%–30% relative to WT (Figure S6B). On PNAd^{+}CD34 and ICAM1, Rasa3/Sipa1-KO T cells were spontaneously arrested with frequencies comparable with those of WT in the presence of CCL21 (Figure 4B). The total adhesive events were also increased by approximately 50%, suggesting that LFA1/ICAM1 interactions augmented the capturing events rather than converting from rolling to arrest in Rasa3/Sipa1-KO T cells. Interestingly, Rasa3/Sipa1-KO T cells exhibited short rolling and arrest on ICAM1 alone under low-shear conditions (2 dyn/cm^2) (Figure 4C). The rolling and arrest of Rasa3/Sipa1-KO T cells on ICAM1 were almost abolished by the absence of talin1 (Figure 4C). Since conformation/affinity changes of LFA1 are involved in rolling and arrest,[8,10] affinity changes of LFA1 in mutant T cells were measured using soluble ICAM1-Fc. Rasa3/Sipa1-KO T cells did not show significant binding to soluble ICAM1-Fc in buffer containing Ca^{2+} and Mg^{2+} but exhibited 2-fold greater binding than WT T cells in the presence of Mn^{2+} (Figure 4D). The impact of Mn^{2+} on ligand-binding affinity was abolished by the absence of Rap1 (Figure 4D). This finding suggests that increased inside-out signaling is required but not sufficient for affinity upregulation of LFA1, for which conformational changes of the ectodomains induced by Mn^{2+} or binding to ICAM1 on the membrane might also be necessary. To confirm this possibility, we measured the binding affinity of LFA1 to ICAM1 presented on planar lipid bilayers. Single-molecule imaging of diffusing ICAM1 on supported lipid bilayers enabled us to detect LFA1-ICAM1 interactions due to a reduction in lateral mobility of LFA1-bound ICAM1 by two orders of magnitude compared with freely mobile ICAM1.[19,22] As expected, WT T cells minimally adhered to ICAM1 on the membrane, but Rasa3/Sipa1-KO T cells spontaneously attached to ICAM1 on the membrane even under Ca^{2+}/Mg^{2+} conditions. The frequency of LFA1-ICAM1 binding of Rasa3/Sipa1-KO T cells was significantly higher than that of WT (Figure 4E, left panel). Moreover, events with a binding time longer than 1 s for Rasa3/Sipa1-KO T cells were significantly more frequent than those of WT (Figure 4E, middle). The dissociation rate constant (k_{off}) of Rasa3/Sipa1-KO T cells, determined from stable binding lifetimes and frequencies of LFA1-ICAM1 interactions, was 0.030 s^{-1}, which was comparable with that of high-affinity LFA1,[48] whereas k_{off} for WT T cells was 0.398 s^{-1}, representing an almost 10-fold shorter lifetime than KO T cells (Figure 4E, right). These results indicate that constitutively activated Rap1 facilitates conversion from low-affinity LFA1 to high-affinity LFA1 for membrane-anchored ICAM1.

Distinct effects of RapGAP deficiencies on rolling and arrest by α4β7

The loss of Rasa3/Sipa1 similarly increased shear-resistant attachment to MAdCAM1, which was also abolished by Rap1 and talin1 deficiency (Figure 5A). Strikingly, however, the capture events of Rasa3/Sipa1-KO T cells on MAdCAM1 under flow conditions were severely reduced compared with those of WT (Figure 5B), which was attributed mainly to decreases in tether and rolling (Figure S6C). The absence of talin1 increased rolling, but not arrest, with the total capture events comparable with those of WT (Figures 5C, and S6D). This corresponds with the results showing that rolling of α4β7 did not require Rap1 and integrin adaptors (Figure 2). Importantly, soluble binding assays using MAdCAM1-Fc showed that ligand-binding affinity of α4β7 in Ca^{2+}/Mg^{2+} buffer increased in Rasa3/Sipa1-KO T cells (Figure 5D). Mn^{2+} increased MAdCAM1-Fc-binding in WT T cells, which was comparable with that of mutant T cells and not affected by Rap1 deficiency (Figures 5D, and S6E). Thus, unlike LFA1, increased Rap1 activation alone induced affinity upregulation of α4β7, which was inhibitory for under-flow adhesion. Collectively, these findings demonstrated the critical importance of the sequential outside-in/inside-out signaling for α4β7 activation in flow conditions.

DISCUSSION

Here we showed the relative contributions of Rap1, kindlin-3, and talin1 to lymphocyte homing as well as rolling and arrest. Compared with the severe homing defects to peripheral LN of Rap1- or talin1-deficient T cells, kindlin-3-deficient T cells were normally attached via LFA1 to relatively large HEVs at branching order III, but fewer are attached to small high-shear HEVs. Kindlin-3 was not essential for *in vitro* adhesion at high-density ICAM1. Thus, these results support the notion that kindlin-3 is important for high-affinity adhesion to low-density ligands or adhesion under high shear stress.[8,19,40]

Previous studies showed that extended LFA1 with the intermediate-affinity I domain support rolling on ICAM1.[5,6] LFA1 in T cells failed to mediate rolling adhesion to ICAM1, even at high ligand densities and low-shear flow. However, interactions of LFA1 and ICAM1 increased L-selectin-dependent capture frequencies and lowered rolling velocities on $PNAd^{+}CD34$ and ICAM1. Localization of L-selectin and LFA1 on tips of lymphocyte microvilli likely enable their functional cooperation in flow conditions.[49] Rap1 or talin1 deficiency abrogated rolling support by LFA1, while the contribution of kindlin-3 to rolling was marginal. These results are in line with a previous study showing that neutrophil slow rolling is mediated by extended, intermediate-affinity LFA1 that requires talin1 but not kindlin-3.[8] However, the molecular mechanism for lymphocyte slow rolling seems to be different from neutrophils. In neutrophils, LFA1 activation is mediated through E-selectin-engaged PSGL-1 that forms a complex with L-selectin. The signaling pathway requires the cytoplasmic tail of L-selectin[50] as well as signaling components of ITAM-containing adaptor proteins, SRC family kinases, PLCγ2, and RasGRP2.[51,52]

Rolling by L-selectin and $PNAd^{+}CD34$ showed a small Rap1 activation in T cells, suggesting that engaged L-selectin could activate Rap1. The absence of Rap1, however, did not affect rolling. In contrast, the addition of ICAM1 induced greater Rap1 activation accompanied by increased capture frequencies and deceleration of rolling. Our results

indicate that the outside-in signaling of LFA1 and ICAM1 made a major contribution to Rap1 activation through RasGRP2 and C3G. In this context, we showed talin1 was also necessary for Rap1 activation that occurred at the initiation of slow rolling of T cells. Furthermore, imaging of talin1 revealed accumulation of talin1 also occurred concomitant with slow rolling. Thus, our study provides direct evidence to support the notion that bidirectional regulation of LFA1 with simultaneous binding of ICAM1 and talin1 under shear flow increase subsecond Rap1 activation and induce extended intermediate-affinity conformations of LFA1, resulting in increasing the capture and stabilizing the rolling. Chemokine stimulation induces recruitment of kindlin-3 as well as talin1 to the β2 cytoplasmic tail of ICAM1-bound LFA1,[19] which likely promotes a shift to high-affinity conformations that mediate arrest (Figure 6A).

Deficiency in both Rasa3 and Sipa1 in T cells resulted in constitutive Rap1 activation and increased frequencies of spontaneous arrest without chemokines. Indeed, single-molecule measurements of mutant T cells on binding to membrane-anchored ICAM1 demonstrated high-affinity LFA1-ICAM1 interactions. However, Rap1 activation alone did not induce apparent affinity changes of LFA1. Therefore, increased activated Rap1 is required but not sufficient for affinity upregulation of LFA1, for which membrane-anchored ICAM1 is necessary. Since binding to immobilized ICAM1 under shear flow accelerates conformational/affinity changes of LFA1 by the tensile force exerted on LFA1,[10,53] increased basal Rap1 activation renders mechanosensitive LFA1 more responsive to ligand binding in shear flow, leading to activation and arrest without chemokines.

Unlike LFA1, α4β7 mediated rolling in the absence of Rap1 and integrin adaptors. These findings indicate that tether/rolling through α4β7 is regulated by unique intrinsic ligand-binding properties, and not by Rap1 and integrin adaptors. Crystal and electron microscopy (EM) studies have demonstrated structural specializations of α4β7, exhibiting a less compact conformation with a unique intermediate conformation of the headpiece, besides closed or open headpiece.[54] The intermediate headpiece conformation is thought to be attributed to rolling adhesion by α4β7.[54] Our findings support this notion and further indicate that the specialized structural features enable α4β7 to mediate rolling independent of inside-out signaling and integrin adaptors (Figure 6B).

Notably, the impacts of constitutive Rap1 activation on α4β7 due to deficiencies of both Rasa3 and Sipa1 were quite different from LFA1: high levels of activated Rap1 suppressed all adhesive events of T cells to MAdCAM1 under shear flow, despite induction of strong adhesion to MAdCAM1 in non-flow conditions. Unlike LFA1, the highly activated Rap1 converted conformations of α4β7 to those with higher affinities, as shown by using soluble ligand-binding assays. High-affinity α4β7 is suitable for firm arrest due to slower on and off rates of ligand binding, rather than rolling-supportive conformations with higher on/off rates.[55] Thus, a prior formation of high-affinity conformations would not be suitable for tether/rolling by α4β7 due to slow rates under flow, leading to a failure of downstream adhesive events. Talin1 deficiency rescued tether/rolling but arrested adhesion, confirming this notion.

Our work demonstrated distinct bidirectional regulation of LFA1 and α4β7 by ligands, Rap1, and integrin adaptors in T cells under shear flow. Simultaneous occupancy with ICAM1 and talin1 across the plasma membrane is required for LFA1 activation, which results in rolling or arrest dependent on Rap1 activation levels. In contrast, sequential activation of α4β7 by outside-in and inside-out signaling is important for efficient arrest (Figure 6). Our findings provide a framework for understanding of the bidirectionality of integrin regulation as well as important information for the development of therapeutics for integrin-involved pathological disorders.

Limitations of the study

Our study has revealed the distinct impacts on affinity of LFA1 and α4β7 by activated Rap1, generating promotion or suppression of adhesion in flow conditions. The distinct outcomes of *in vitro* adhesion responses of T cells should be investigated further *in vivo*. In particular, the *in vivo* effects of high basal Rap1 activities on T cell trafficking should be explored in detail. Other intracellular components, including RIAM and its paralog lamellipodin, likely play important roles in the cell-specific regulation of talin1. Future work warrants elucidating the molecular mechanisms underlying the unique properties of bidirectional regulation by integrin adaptors, Rap1, and its effectors.

STAR★METHODS

RESOURCE AVAILABILITY

Lead contact—Further information should be directed to and will be fulfilled by the lead contact, Tatsuo Kinashi (kinashi@hirakata.kmu.ac.jp).

Materials availability—Requests for resources and reagents should be directed to and will be fulfilled by the lead contact.

Data and code availability

- Original cell tracking data and microscopy data in our manuscript will be shared by the lead contact upon request.
- All original MATLAB code will be shared by the lead contact upon request.
- Any additional information required to reanalyze the data reported in this paper is available from the lead contact upon request.

EXPERIMENTAL MODEL AND SUBJECT DETAILS

Animals—C57BL/6 mice were obtained from CLEA Japan. *Cd4-cre* transgenic mice on a C57BL/6 background were obtained from Taconic and used for T cell–specific conditional knockout mice. *Rap1a*$^{f/f}$; *Rap1b*$^{f/f}$ mice were described.[25] *Talin1*$^{f/f}$ mice were obtained from EUCOMM (Tln1tm4.1Crit).[58] Conditional kindlin-3 knockout mice (*Fermt3*$^{f/f}$) were generated using an ES cell line (*Fermt3tm1a*(*KOMP)Wtsi*) obtained from KOMP. Conditional C3G or RasGRP2 knockout mice were generated (Figure S4). *Rasa3*$^{f/f}$ and *Itga1*$^{-/-}$ mice were described previously.[56,59] *Sipa1*$^{-/-}$ mice were generated by CRISPR-Cas9 with a guide RNA targeted for exon7 of *sipa1* (Y.U., K. Higasa, Y.K., N.K., S.

Horitani, Y.I., W.B., Y. Fukui, and T.K., unpublished data). HaloTag-Talin1 (HT-Tln1) knockin mice were generated by CRISPR-Cas9 system. All transgenic mice were on a C57BL/6 background and crossed with *Cd4-cre* mice for T-cell–specific deletion of floxed genes. Bone marrow cells from *Cd4-cre; Rasa3*$^{f/f}$; *Sipa1*$^{-/-}$; *Rap1a*$^{f/f}$; *Rap1b*$^{f/f}$ mice were transplanted into gamma-ray (10 Gy) irradiated mice to increase the number of the mutants as well as control mice. Mice were maintained under specific pathogen-free conditions in the animal facility at Kansai Medical University. For experiments, 7- to 25-week-old mice were used. Both male and female mice were used. In the transplant experiments, donors and recipients were same-sex. All animal experiments were performed following protocols approved by the Animal Care and Use Committee of Kansai Medical University (approval no. 21–082(04)).

Cell culture—T cells were isolated from spleens with Mojosort Mouse CD3 T cell Isolation Kit (Biolegend) with some modifications. The preparation of T cells took place at room temperature (RT) with an IMDM medium containing 1% FBS, 2-ME, and penicillin/streptomycin (P/S). In some experiments, effector T cells (CD44^{hi}) were depleted as follows: 10 μg of anti-CD44 conjugated with biotin was mixed with 200 μL of magnetic beads suspension (Biolegend) at room temperature for 10 min; magnetic beads were centrifuged at 12000 rpm for 10 min; supernatants were removed, magnetic beads were dissolved in 200 μL of PBS (CD44-depletion beads); for 2×10^7 purified Tln-KO or Rap1-KO T cells, 50 μL of CD44-depletion beads were incubated for 15 min at room temperature. For WT T cells, 25 μL of CD44-depletion beads were incubated; magnetic isolation was performed twice. Single-cell suspensions were stained with fluorophores-conjugated Abs by direct or indirect methods. Fluorescence-activated cell sorting (FACS) data were acquired using a FACSCalibur, FACSCanto II (BD Biosciences), or Attune Nxt (Thermo Fisher Scientific) and analyzed with CellQuest or FlowJo (BD Biosciences). Cultured T cells were prepared with stimulation with anti-CD3 and anti-CD28 antibodies in the presence of human IL-2 (Peprotech) as described.[22] For Tln-KO T blast culture, 10 ng/mL of PMA was added from day 0 to day 2 at 37°C.

METHOD DETAILS

Antibodies and reagents—The following antibodies (Abs) labeled with fluorophores or biotin were purchased from Biolegend: B220 (clone RA3–6B2), CD3 (2C11), CD62L/L-selectin (MEL-14), integrin αL (M17/4), α4β7 (DATK32), CD4 (GK1.5), CD8 (53–6.7), CD44 (IM7), and CD45 (30-F11). Anti-PNAd (MECA-79), 4-chloromethyl-6,8-difluoro-7-hydroxycoumarin (CMF_2HC), 5,6-carboxyfluorescein diacetate (CFSE), 5-(and-6)-(((4-chloromethyl)benzoyl)amino) tetramethylrhodamine (CMTMR), and IMDM medium were purchased from Thermo Fisher Scientific. Monoclonal Abs against αL (KBA), ICAM1 (YN1/1.7.4), MAdCAM1 (MECA-89), and L-selectin (MEL-14) were purified from supernatants of hybridomas (ATCC) for blocking experiments or flow cytometric analysis. Mouse MAdCAM1-Fc chimera was purchased from R&D Systems. Anti-human IgG Fc (Rockland) was used for capturing Ab and western blotting. Anti-human CD34 was purchased from Santa Cruz. Recombinant CCL21 was purchased from R&D systems. Anti-kindlin1 (22215–1-AP) and anti-kindlin2 (11453–1-AP) were purchased from Proteintech.

Anti-kindlin3 (ab68040) was purchased from Abcam. Anti-alpha tubulin (clone DM1a) and anti-talin1/2 (clone 8d4) were purchased from Merk.

***In vivo* short homing assay—**Purified T cells from spleens of control or knockout mice were labeled with 25 μM CMF_2HC, 0.5 μM CFSE, or 1 μM CMTMR, respectively. An equal number of labeled cells (1×10^7 each) were injected intravenously into WT mice. After 1 h, labeled T cells were harvested from spleen, surface (inguinal and auxiliary) LN, mesenteric LN, and Peyer's patches and were analyzed by flow cytometry to detect transferred cells. The ratio against control T cells in tissues was calculated as homing efficiency in which raw data was compensated by the ratio of input cells. The reversal of the fluorescent dyes produced the same results. To exclude the effect of dyes, we also performed control experiments with differently labeled WT T cells (Figure S1C).

Analysis of transferred T cellT-cell distribution in HEV—Purified T cells from control or mutant mice were labeled with 75 μM CMF_2HC and 1 μM CMTMR, respectively. An equal number of labeled cells were injected intravenously into a normal C57BL/6 mouse. Twenty-five minutes after cell injection, HEVs were labeled by intravenous injection of Alexa Fluor 488-MECA-79 for 5 min. Peripheral (inguinal and auxiliary) LNs were collected from sacrificed mice and fixed with 4% PFA in PBS. LNs were sliced using a vibratome with 300 μm thickness. Both sides of the LN slices were imaged by a confocal microscope FV3000 (Olympus) equipped with a UPLSAPO10×2 objective. The relative fractions of mutant and control T cells attached to order III-V HEVs were measured. For the control experiment, dyes were swapped. For the blocking experiment, input cells were treated with 100 μg/mL anti-mouse integrin αL at 37°C for 30 min.

Analysis of transferred T cellT-cell distribution in spleen—CFSE-labeled T cells from WT mice and CMTMR-labeled T cells from knockout mice were prepared as same as short homing assay. An equal number of labeled cells (1×10^7 each) were injected intravenously into WT mice. The initial input ratio (CMTMR/CFSE) of the cell mixture was analyzed by FACS. After 1 h, spleens were extracted from sacrificed mice, and fixed with 4% paraformaldehyde (PFA) in PBS for more than 10 h. PFA-fixed spleens were sliced with 300 μm thickness by vibratome. Sliced spleens were permeabilized with 0.1% Triton X-100 in PBS for more than 1 h and blocked with 0.1% Triton X-100, 1% BSA, 1% rat serum in PBS for more than 5 h. After the blocking, slices were labeled with anti-B220 conjugated with eFluor450 (2 μg/mL) and anti-CD3 conjugated with APC (2 μg/mL) for more than 10 h followed by three-times washing with 0.1% Triton X-100 for 30 min. Confocal images were obtained by FV3000 with 10× lens. Images were analyzed by using a plug-in Analyze Particles program of Fiji. Transferred cells in white pulp were defined by the fluorescence brightness and size in APC-$CD3^+$ area. Total cell area of each color (μm^2) was calculated because counting of cell number was difficult due to the overlap of multiple cells. Percentage to CFSE control was calculated by relative ratio of each area (CMTMR/CFSE) normalized by the initial input ratio.

Fc chimeras—The extracellular domains of human CD34 were cloned into a pIG vector[57] to generate human IgG Fc chimera.[44] To obtain glycosylated CD34, the expression vector

was introduced into LS12 cells stably expressing α−1,3-fucosyltransferase (Fuc-T VII) and N-acetylglucosamine 6-O-sulfotransferase (6-Sul-T).[44] The glycosylated CD34-Fc was purified from the culture supernatants by using protein G Sepharose 4FF column (GE healthcare). Mouse ICAM1-Fc was purified from a culture supernatant of 293T cells transfected with their expression vectors. Mouse MAdCAM1-Fc was purchased from R&D Systems.

Quantification of site densities of coated proteins—The chloramine-T iodination procedure[60] was used for ^{125}I-labeling of antibodies (YN1/1.7.4 for ICAM1, MECA-89 for MAdCAM1, and MECA-79 for PNAd). Carrier-free Na^{125}I (NEZ033A) was purchased from PerkinElmer. Purified antibodies (100 μL, 1 mg/mL), 0.5 mCi ^{125}I, and 10 μL of chloramine T (1 mg/mL in PBS) were mixed and incubated for 2–4 min at room temperature. The reaction was stopped by the addition of 10 μL of sodium metabisulfite (2 mg/mL) and 20 μL of NaI (1% w/v). Iodinated antibodies were isolated with a size-exclusion column (PD-10, #17–0851-01, Cytiva). The specific activities of labeled proteins were determined by measuring ^{125}I incorporation. The site densities of Fc proteins coated on polystyrene disks were measured by overlaid experiments with saturated amounts of iodinated antibodies. After washing, bound antibodies were eluted for counting. The site density was determined using specific activities of iodinated antibodies shown in Figure S2A.

Detachment and flow adhesion assays using shear stress—Detachment assays were performed using a temperature-controlled parallel-plate flow chamber (FCS2, Bioptechs) at 37°C. Laminar shear stress was determined by using an equation of shear stress, $6Q\mu/wh^2$ (dyn/cm^2), in which symbols denote the following: Q, flow rate (mL/min); m, viscosity (0.007 P for buffer); w, chamber width (1.2 cm); h, chamber height (0.1 mm).[61] For coating with ligands, capture antibodies were coated on the center of polystyrene disks, then washed and overlaid with recombinant mouse PNAd$^+$CD34-Fc, ICAM1-Fc, or MAdCAM1-Fc. For coating with both PNAd$^+$CD34-Fc and ICAM1-Fc, PNAd$^+$CD34-Fc was coated before ICAM1-Fc. For some experiments, CCL21 (200 nM in PBS) was also coated at room temperature for 30 min after blocking. Purified T cells (2×10^6/mL) were suspended in a warm medium (IMDM containing 1% FBS) and loaded into the chamber, and bright-field images were recorded every 5 s with a 4× objective lens and CCD camera (HAMAMATSU C2741). After cells were settled on the coated substrates for 5 min, shear stress was applied for 1 min at 2 dyn/cm^2 with a stepwise increment of 1 dyn/cm^2 every minute to 5 dyn/cm^2 using a programmed syringe pump (FP-1000, MELQUEST). The attached cells were counted at the end of each shear stress by using an Integrated Morphometry Analysis program of Metamorph (Molecular Devices). Adhesion efficiencies were percentages of attached cell numbers relative to input cell numbers.

For flow adhesion assays, the ligands' coating was essentially the same as that in detachment assays, with modifications. The upstream part of the disk was masked by a silicon rubber for measurement of cell influx in the flow. Influx and captured cells (tether/rolling/arrest) were counted in the influx area (0.78 mm^2) and the capture area (1.05 mm^2), respectively, during the same 1000 frames of the imaging period (33.3 s), and normalized for time and area

(cell numbers/sec/mm^2). Cell accumulation index, a relative degree of cell accumulation in the capture area relative to that in the influx area were calculated by dividing normalized captured cell numbers by normalized influx cell numbers. For tracking of adhesive events of T cells on the capture area, we employed a plugin program TrackMate (ver.5.0.2) for a Fiji program with parameters adjusted for displacement rates of cells below those of flowing cells. Position data (x, y, t) of trajectories were further analyzed with MATLAB (MathWorks). Moving and stopping of cells were defined with threshold displacement rates of 1 μm/frame and 0.5 μm/frame in 100 consecutive frames on PNAd$^+$CD34/ICAM1 and MAdCAM1, respectively, to distinguish arrest from rolling. Adhesive events longer than 1 s were analyzed and categorized as follows: tether (1–3.3 s stopping), arrest (>3.3 s stopping), and rolling (moving >1 s). Only the first trajectory of the same cell was analyzed. Capture events (tether, arrest, or rolling) were normalized with time, area, and cell influx (cell numbers/second/mm^2). Relative capture frequencies were defined as normalized capture events relative to those of the wild-type control. Average rolling velocities were calculated using displacement and duration longer than 1 s.

Measurement of Rap1 activity under flow conditions—To measure Rap1 activities in T cells, an affinity probe for Rap1-GTP (RalGDS-RBD-GFP) was introduced via a lentivirus as described previously.[22,25] Infected T blasts were expanded with IL-2 for 5–6 days and sorted for cells expressing the affinity probe moderately. Cells were maintained in IMDM containing 1% FBS for 6–7 h for starvation. Cell debris was removed by centrifugation using Lympholyte M (Cedarlane Laboratories) and subjected to flow adhesion assays described below. Fluorescence images (1024 × 1024 pixels) were acquired at 52.6 fps with a UPLSAPO10×2 objective lens, and an inverted IX-83 microscope (Olympus) equipped with a CMOS camera (ORCA-Flash4.0V3 HAMAMATSU) and a white-light LED (X-Cite XYLIS, Excelitas) for excitation. Acquired images were processed for background and cell tracking. The coordinates (x, y), mean intensities, and displacements of the object were obtained by using a plug-in Analyze Particles program of Fiji (https://imagej.net/software/fiji/) and used for the plot of intensities and displacement against time. The time point at which a cell initiates the tether/rolling was set to zero. The mean intensities were normalized at time zero.

Measurement of talin1 accumulation under flow conditions—Purified splenic T cells from HaloTag-talin1 knockin mice were labeled with 1μ M SaraFluor650T ligand (Goryo chemical) in IMDM medium containing 4% FBS, 2-ME and P/S at 37°C for 60 min. After the medium change and wash culture at 37°C more than 30 min, cells were subjected to flow adhesion assays described above. Fluorescence images (1024 × 1024 pixels) were acquired at 34.5 fps with a UPlanApo20X objective lens, and an inverted IX-83 microscope equipped with a CMOS camera and a white-light LED for excitation. Acquired images were processed for background and cell tracking. The coordinates (x, y), mean intensities, and displacements of the object were obtained by using a plug-in Analyze Particles program of Fiji and used for the plot of intensities and displacement against time. The time point at which a cell initiates the tether/rolling was set to zero. The mean intensities were normalized (as 100%) at time zero as same as the Rap1 activity imaging.

Western blotting—Western blotting was performed as described[25] by using the LAS3000mini image analyzer (FUJIFILM) or Odyssey image analyzer (LI-COR). Talin2 was not detected in Tln-KO T cells by using anti-Talin1/2 by western blotting.

Rap1 pull-down assay—Isolated T cells were stimulated with CCL21 for 5 s and immediately lysed with 2× lysis buffer (0.2% Triton X-, 300 mM NaCl, 100 mM Tris-HCl, and 20 mM $MgCl_2$). Then, the samples were subjected to Rap1 pull-down assays using glutathione Sepharose beads (Cytiva) conjugated with GST-RalGDS-RBD, followed by immunoblotting with anti-Rap1 antibodies (BD Bioscience). Rap1 pull-down assay was performed as described previously.[25]

Soluble ligand binding assays—Purified T cells were washed with saline buffer containing 20 mM HEPES (pH 7.4), 140 mM NaCl, and 2 mg/mL glucose, and resuspended (1×10^6/25 μL) in the same buffer supplemented with EDTA (5 mM), $CaCl_2$ and $MgCl_2$ (0.5 mM for each), or $MnCl_2$ (1 mM), and mixed with ICAM1-Fc or MAdCAM1-Fc to a final concentration of 0.1 μM. Cells were incubated at 37°C for 30 min. After the incubation, cells were fixed with pre-warmed 2% PFA/HBSS buffer for 5 min and washed with HBSS containing 0.5% BSA twice, then incubated with Aelxa488-anti-human IgG and subjected to flow cytometric analysis. Median fluorescence intensity (MFI) was normalized with the Fc chimeric protein-free conditions.

Single-molecule imaging of LFA1-ICAM1 interactions—Measurements of binding kinetics of LFA1 and ICAM1 were performed as described in our previous studies.[19,22] Briefly, mouse ICAM1-GPI was purified, labeled with ATTO647N-NHS-ester, and incorporated into liposomes consisting of 0.4 mM 1,2-dioleoyl-sn-glycero-3-phosphocholine containing 0.1 mol% 1,2-dioleoyl-sn-glycero-3-phosphoethanolamine-N-(cap biotinyl) (sodium salt) (Avanti Polar Lipids). Liposomes harboring ICAM1-GPI were applied onto piranha-treated cover glass to generate supported planar lipid bilayers presenting ICAM1. Single-molecule binding events between LFA1 and ICAM1 on primary T cells (WT or Rasa3/Sipa1-KO) were recorded at 33-msec intervals on a total internal reflection microscope (TIRFM, Olympus) in the buffer containing 20 mM HEPES (pH 7.4), 140 mM NaCl, 2 mg/mL glucose, 0.5 mM $CaCl_2$, and 0.5 mM $MgCl_2$. When bound to LFA1, rapidly moving ICAM1 decelerated or arrested, exhibiting diffusion coefficients two orders of magnitude smaller than unbound ICAM1. Single-particle tracking of ICAM1 was performed using the G-count and G-track software (G-angstrom). Frequencies and bond lifetimes extracted from trajectories of bound ICAM1 were used for the calculation of dissociation rate constants.[22]

Interference reflection microscopy (IRM)—Measurements of adhesion area and analysis were performed as described in our previous studies.[19,22]

QUANTIFICATION AND STATISTICAL ANALYSIS

GraphPad Prism software (GraphPad) or Excel (Microsoft) were used for statistical analyses. The means of the two groups were compared with a Student's t-test or paired t test. A Chi-square test was performed for analyzing relative capture frequencies (rolling/

tether/arrest) by multiplying the percentage by a hundred. *p < 0.05, **p < 0.01, ***p < 0.001, and n.s., not significant.

Supplementary Material

Refer to Web version on PubMed Central for supplementary material.

ACKNOWLEDGMENTS

We thank Manami Nishimura, Rie Hamaguchi, Keiko Kawai, and Akiko Kawasaki (Kansai Medical University) for technical assistance and support. This study was supported by JSPS KAKENHI grant number 25291047 (to T.K.), 22H02623 (to T.K.), 17K08796 (to Y.K.), 17H05516 (to Y.K.), 21K06181 (to Y.K.), a Grant-in-Aid for Scientific Research on Innovative Areas 22111003 (to T.K.), and a Private University Research Branding Project on Intractable Immune and Allergic Diseases grant from Kansai Medical University and NIH grant R35 HL144976 (to W.B.).

REFERENCES

1. Butcher EC, and Picker LJ (1996). Lymphocyte homing and homeostasis. Science 272, 60–66. [PubMed: 8600538]
2. Springer TA (1994). Traffic signals for lymphocyte recirculation and leukocyte emigration: the multistep paradigm. Cell 76, 301–314. 10.1016/0092-8674(94)90337-9. [PubMed: 7507411]
3. von Andrian UH, and Mempel TR (2003). Homing and cellular traffic in lymph nodes. Nat. Rev. Immunol 3, 867–878. 10.1038/nri1222nri1222[pii]. [PubMed: 14668803]
4. Ley K, Laudanna C, Cybulsky MI, and Nourshargh S (2007). Getting to the site of inflammation: the leukocyte adhesion cascade updated. Nat. Rev. Immunol 7, 678–689. [PubMed: 17717539]
5. Salas A, Shimaoka M, Kogan AN, Harwood C, von Andrian UH, and Springer TA (2004). Rolling adhesion through an extended conformation of integrin alphaLbeta2 and relation to alpha I and beta I-like domain interaction. Immunity 20, 393–406. [PubMed: 15084269]
6. Salas A, Shimaoka M, Phan U, Kim M, and Springer TA (2006). Transition from rolling to firm adhesion can be mimicked by extension of integrin alphaLbeta2 in an intermediate affinity state. J. Biol. Chem 281, 10876–10882. [PubMed: 16505487]
7. Sigal A, Bleijs DA, Grabovsky V, van Vliet SJ, Dwir O, Figdor CG, van Kooyk Y, and Alon R (2000). The LFA-1 integrin supports rolling adhesions on ICAM-1 under physiological shear flow in a permissive cellular environment. J. Immunol 165, 442–452. 10.4049/jimmunol.165.1.442. [PubMed: 10861083]
8. Lefort CT, Rossaint J, Moser M, Petrich BG, Zarbock A, Monkley SJ, Critchley DR, Ginsberg MH, Fässler R, and Ley K (2012). Distinct roles for talin-1 and kindlin-3 in LFA-1 extension and affinity regulation. Blood 119, 4275–4282. 10.1182/blood-2011-08-373118. [PubMed: 22431571]
9. Luo BH, Carman CV, and Springer TA (2007). Structural basis of integrin regulation and signaling. Annu. Rev. Immunol 25, 619–647. 10.1146/annurev.immunol.25.022106.141618. [PubMed: 17201681]
10. Shamri R, Grabovsky V, Gauguet JM, Feigelson S, Manevich E, Kolanus W, Robinson MK, Staunton DE, von Andrian UH, and Alon R (2005). Lymphocyte arrest requires instantaneous induction of an extended LFA-1 conformation mediated by endothelium-bound chemokines. Nat. Immunol 6, 497–506. 10.1038/ni1194. [PubMed: 15834409]
11. Li J, and Springer TA (2018). Energy landscape differences among integrins establish the framework for understanding activation. J. Cell Biol 217, 397–412. 10.1083/jcb.201701169. [PubMed: 29122968]
12. Moser M, Bauer M, Schmid S, Ruppert R, Schmidt S, Sixt M, Wang HV, Sperandio M, and Fässler R (2009). Kindlin-3 is required for beta2 integrin-mediated leukocyte adhesion to endothelial cells. Nat. Med 15, 300–305. [PubMed: 19234461]
13. Sun Z, Costell M, and Fässler R (2019). Integrin activation by talin, kindlin and mechanical forces. Nat. Cell Biol 21, 25–31. 10.1038/s41556-018-0234-9. [PubMed: 30602766]

14. Wen L, Moser M, and Ley K (2022). Molecular mechanisms of leukocyte beta2 integrin activation. Blood 10.1182/blood.2021013500.
15. Alon R, and Ley K (2008). Cells on the run: shear-regulated integrin activation in leukocyte rolling and arrest on endothelial cells. Curr. Opin. Cell Biol 20, 525–532. 10.1016/j.ceb.2008.04.003. [PubMed: 18499427]
16. Hogg N, Patzak I, and Willenbrock F (2011). The insider's guide to leukocyte integrin signalling and function. Nat. Rev. Immunol 11, 416–426. 10.1038/nri2986. [PubMed: 21597477]
17. Schürpf T, and Springer TA (2011). Regulation of integrin affinity on cell surfaces. EMBO J 30, 4712–4727. 10.1038/emboj.2011.333. [PubMed: 21946563]
18. Calderwood DA, Campbell ID, and Critchley DR (2013). Talins and kindlins: partners in integrin-mediated adhesion. Nat. Rev. Mol. Cell Biol 14, 503–517. 10.1038/nrm3624. [PubMed: 23860236]
19. Kondo N, Ueda Y, and Kinashi T (2021). Kindlin-3 disrupts an intersubunit association in the integrin LFA1 to trigger positive feedback activation by Rap1 and talin1. Sci. Signal 14, eabf2184. [PubMed: 34103420]
20. Kinashi T (2005). Intracellular signalling controlling integrin activation in lymphocytes. Nat. Rev. Immunol 5, 546–559. 10.1038/nri1646. [PubMed: 15965491]
21. Stadtmann A, Brinkhaus L, Mueller H, Rossaint J, Bolomini-Vittori M, Bergmeier W, Van Aken H, Wagner DD, Laudanna C, Ley K, and Zarbock A (2011). Rap1a activation by CalDAG-GEFI and p38 MAPK is involved in E-selectin-dependent slow leukocyte rolling. Eur. J. Immunol 41, 2074–2085. 10.1002/eji.201041196. [PubMed: 21480213]
22. Kondo N, Ueda Y, Kita T, Ozawa M, Tomiyama T, Yasuda K, Lim DS, and Kinashi T (2017). NDR1-Dependent regulation of kindlin-3 controls high-affinity LFA-1 binding and immune synapse organization. Mol. Cell Biol 37, e00424. [PubMed: 28137909]
23. Ishihara S, Nishikimi A, Umemoto E, Miyasaka M, Saegusa M, and Katagiri K (2015). Dual functions of Rap1 are crucial for T-cell homeostasis and prevention of spontaneous colitis. Nat. Commun 6, 8982. [PubMed: 26634692]
24. Su W, Wynne J, Pinheiro EM, Strazza M, Mor A, Montenont E, Berger J, Paul DS, Bergmeier W, Gertler FB, and Philips MR (2015). Rap1 and its effector RIAM are required for lymphocyte trafficking. Blood 126, 2695–2703. 10.1182/blood-2015-05-644104. [PubMed: 26324702]
25. Ueda Y, Kondo N, Ozawa M, Yasuda K, Tomiyama T, and Kinashi T (2016). Sema3e/Plexin D1 Modulates Immunological Synapse and Migration of Thymocytes by Rap1 Inhibition. J. Immunol 196, 3019–3031. 10.4049/jimmunol.1502121. [PubMed: 26921307]
26. Sun H, Lagarrigue F, Wang H, Fan Z, Lopez-Ramirez MA, Chang JT, and Ginsberg MH (2021). Distinct integrin activation pathways for effector and regulatory T cell trafficking and function. J. Exp. Med 218, e20201524. [PubMed: 33104169]
27. Crittenden JR, Bergmeier W, Zhang Y, Piffath CL, Liang Y, Wagner DD, Housman DE, and Graybiel AM (2004). CalDAG-GEFI integrates signaling for platelet aggregation and thrombus formation. Nat. Med 10, 982–986. [PubMed: 15334074]
28. Gutierrez-Herrero S, Fernandez-Infante C, Hernandez-Cano L, Ortiz-Rivero S, Guijas C, Martin-Granado V, Gonzalez-Porras JR, Balsinde J, Porras A, and Guerrero C (2020). C3G contributes to platelet activation and aggregation by regulating major signaling pathways. Signal Transduct. Targeted Ther 5, 10.
29. Kloog Y, and Mor A (2014). Cytotoxic-T-lymphocyte antigen 4 receptor signaling for lymphocyte adhesion is mediated by C3G and Rap1. Mol. Cell Biol 34, 978–988. 10.1128/MCB.01024-13. [PubMed: 24396067]
30. Stefanini L, and Bergmeier W (2016). RAP1-GTPase signaling and platelet function. J. Mol. Med. (Limerick) 94, 13–19. 10.1007/s00109-015-1346-3.
31. Hattori M, Tsukamoto N, Nur-e-Kamal MS, Rubinfeld B, Iwai K, Kubota H, Maruta H, and Minato N (1995). Molecular cloning of a novel mitogen-inducible nuclear protein with a Ran GTPase-activating domain that affects cell cycle progression. Mol. Cell Biol 15, 552–560. [PubMed: 7799964]

32. Zhu L, Yang J, Bromberger T, Holly A, Lu F, Liu H, Sun K, Klapproth S, Hirbawi J, Byzova TV, et al. (2017). Structure of Rap1b bound to talin reveals a pathway for triggering integrin activation. Nat. Commun 8, 1744. 10.38/s41467–017-01822–8. [PubMed: 29170462]
33. Song X, Yang J, Hirbawi J, Ye S, Perera HD, Goksoy E, Dwivedi P, Plow EF, Zhang R, and Qin J (2012). A novel membrane-dependent on/off switch mechanism of talin FERM domain at sites of cell adhesion. Cell Res 22, 1533–1545. 10.1038/cr.2012.97. [PubMed: 22710802]
34. Han J, Lim CJ, Watanabe N, Soriani A, Ratnikov B, Calderwood DA, Puzon-McLaughlin W, Lafuente EM, Boussiotis VA, Shattil SJ, and Ginsberg MH (2006). Reconstructing and deconstructing agonist-induced activation of integrin alphaIIbbeta3. Curr. Biol 16, 1796–1806. [PubMed: 16979556]
35. Legate KR, Takahashi S, Bonakdar N, Fabry B, Boettiger D, Zent R, and Fässler R (2011). Integrin adhesion and force coupling are independently regulated by localized PtdIns(4,5)2 synthesis. EMBO J 30, 4539–4553. 10.1038/emboj.2011.332. [PubMed: 21926969]
36. Yago T, Zhang N, Zhao L, Abrams CS, and McEver RP (2018). Selectins and chemokines use shared and distinct signals to activate beta2 integrins in neutrophils. Blood Adv 2, 731–744. 10.1182/bloodadvances.2017015602. [PubMed: 29592875]
37. Hart R, Stanley P, Chakravarty P, and Hogg N (2013). The kindlin 3 pleckstrin homology domain has an essential role in lymphocyte function-associated antigen 1 (LFA-1) integrin-mediated B cell adhesion and migration. J. Biol. Chem 288, 14852–14862. 10.1074/jbc.M112.434621. [PubMed: 23595985]
38. Wen L, Marki A, Roy P, McArdle S, Sun H, Fan Z, Gingras AR, Ginsberg MH, and Ley K (2021). Kindlin-3 recruitment to the plasma membrane precedes high-affinity beta2-integrin and neutrophil arrest from rolling. Blood 137, 29–38. 10.1182/blood.2019003446. [PubMed: 32777822]
39. Chauveau A, Pirgova G, Cheng HW, De Martin A, Zhou FY, Wideman S, Rittscher J, Ludewig B, and Arnon TI (2020). Visualization of T Cell migration in the spleen reveals a network of perivascular pathways that guide entry into T zones. Immunity 52, 794–807.e7. 10.1016/j.immuni.2020.03.010. [PubMed: 32298648]
40. Moretti FA, Klapproth S, Ruppert R, Margraf A, Weber J, Pick R, Scheiermann C, Sperandio M, Fässler R, and Moser M (2018). Differential requirement of kindlin-3 for T cell progenitor homing to the non-vascularized and vascularized thymus. Elife 7, e35816. 10.7554/eLife.35816. [PubMed: 30187863]
41. von Andrian UH (1996). Intravital microscopy of the peripheral lymph node microcirculation in mice. Microcirculation 3, 287–300. 10.3109/10739689609148303. [PubMed: 8930886]
42. Manevich-Mendelson E, Feigelson SW, Pasvolsky R, Aker M, Grabovsky V, Shulman Z, Kilic SS, Rosenthal-Allieri MA, Ben-Dor S, Mory A, et al. (2009). Loss of Kindlin-3 in LAD-III eliminates LFA-1 but not VLA-4 adhesiveness developed under shear flow conditions. Blood 114, 2344–2353. [PubMed: 19617577]
43. Moretti FA, Moser M, Lyck R, Abadier M, Ruppert R, Engelhardt B, and Fässler R (2013). Kindlin-3 regulates integrin activation and adhesion reinforcement of effector T cells. Proc. Natl. Acad. Sci. USA 110, 17005–17010. 10.1073/pnas.1316032110. [PubMed: 24089451]
44. Kimura N, Mitsuoka C, Kanamori A, Hiraiwa N, Uchimura K, Muramatsu T, Tamatani T, Kansas GS, and Kannagi R (1999). Reconstitution of functional L-selectin ligands on a cultured human endothelial cell line by cotransfection of alpha1–>3 fucosyltransferase VII and newly cloned GlcNAcbeta:6-sulfotransferase cDNA. Proc. Natl. Acad. Sci. USA 96, 4530–4535. 10.1073/pnas.96.8.4530. [PubMed: 10200296]
45. Finger EB, Puri KD, Alon R, Lawrence MB, von Andrian UH, and Springer TA (1996). Adhesion through L-selectin requires a threshold hydrodynamic shear. Nature 379, 266–269. 10.1038/379266a0. [PubMed: 8538793]
46. Berlin C, Bargatze RF, Campbell JJ, von Andrian UH, Szabo MC, Hasslen SR, Nelson RD, Berg EL, Erlandsen SL, and Butcher EC (1995). Alpha 4 integrins mediate lymphocyte attachment and rolling under physiologic flow. Cell 80, 413–422. 10.1016/0092-8674(95)90491-3. [PubMed: 7532110]

47. Azoulay-Alfaguter I, Strazza M, Peled M, Novak HK, Muller J, Dustin ML, and Mor A (2017). The tyrosine phosphatase SHP-1 promotes T cell adhesion by activating the adaptor protein CrkII in the immunological synapse. Sci. Signal 10, eaal2880. [PubMed: 28790195]
48. Shimaoka M, Xiao T, Liu JH, Yang Y, Dong Y, Jun CD, McCormack A, Zhang R, Joachimiak A, Takagi J, et al. (2003). Structures of the alpha L I domain and its complex with ICAM-1 reveal a shape-shifting pathway for integrin regulation. Cell 112, 99–111. [PubMed: 12526797]
49. Ghosh S, Feigelson SW, Montresor A, Shimoni E, Roncato F, Legler DF, Laudanna C, Haran G, and Alon R (2021). CCR7 signalosomes are preassembled on tips of lymphocyte microvilli in proximity to LFA-1. Biophys. J 120, 4002–4012. 10.1016/j.bpj.2021.08.014. [PubMed: 34411577]
50. Stadtmann A, Germena G, Block H, Boras M, Rossaint J, Sundd P, Lefort C, Fisher CI, Buscher K, Gelschefarth B, et al. (2013). The PSGL-1-L-selectin signaling complex regulates neutrophil adhesion under flow. J. Exp. Med 210, 2171–2180. 10.1084/jem.20130664. [PubMed: 24127491]
51. Zarbock A, Abram CL, Hundt M, Altman A, Lowell CA, and Ley K (2008). PSGL-1 engagement by E-selectin signals through Src kinase Fgr and ITAM adapters DAP12 and FcR gamma to induce slow leukocyte rolling. J. Exp. Med 205, 2339–2347. 10.1084/jem.20072660. [PubMed: 18794338]
52. Zarbock A, Lowell CA, and Ley K (2007). Spleen tyrosine kinase Syk is necessary for E-selectin-induced alpha(L)beta(2) integrin-mediated rolling on intercellular adhesion molecule-1. Immunity 26, 773–783. 10.1016/j.immuni.2007.04.011. [PubMed: 17543554]
53. Alon R, and Dustin ML (2007). Force as a facilitator of integrin conformational changes during leukocyte arrest on blood vessels and antigen-presenting cells. Immunity 26, 17–27. 10.1016/j.immuni.2007.01.002. [PubMed: 17241958]
54. Yu Y, Zhu J, Mi LZ, Walz T, Sun H, Chen J, and Springer TA (2012). Structural specializations of alpha(4)beta(7), an integrin that mediates rolling adhesion. J. Cell Biol 196, 131–146. 10.1083/jcb.201110023. [PubMed: 22232704]
55. de Château M, Chen S, Salas A, and Springer TA (2001). Kinetic and mechanical basis of rolling through an integrin and novel Ca2+-dependent rolling and Mg2+-dependent firm adhesion modalities for the alpha 4 beta 7-MAdCAM-1 interaction. Biochemistry 40, 13972–13979. 10.1021/bi011582f. [PubMed: 11705388]
56. Schmits R, Kündig TM, Baker DM, Shumaker G, Simard JJ, Duncan G, Wakeham A, Shahinian A, van der Heiden A, Bachmann MF, et al. (1996). LFA-1-deficient mice show normal CTL responses to virus but fail to reject immunogenic tumor. J. Exp. Med 183, 1415–1426. 10.1084/jem.183.4.1415. [PubMed: 8666900]
57. Katagiri K, Hattori M, Minato N, and Kinashi T (2002). Rap1 functions as a key regulator of T-cell and antigen-presenting cell interactions and modulates T-cell responses. Mol. Cell Biol 22, 1001–1015. [PubMed: 11809793]
58. Petrich BG, Marchese P, Ruggeri ZM, Spiess S, Weichert RAM, Ye F, Tiedt R, Skoda RC, Monkley SJ, Critchley DR, and Ginsberg MH (2007). Talin is required for integrin-mediated platelet function in hemostasis and thrombosis. J. Exp. Med 204, 3103–3111. 10.1084/jem.20071800. [PubMed: 18086863]
59. Stefanini L, Paul DS, Robledo RF, Chan ER, Getz TM, Campbell RA, Kechele DO, Casari C, Piatt R, Caron KM, et al. (2015). RASA3 is a critical inhibitor of RAP1-dependent platelet activation. J. Clin. Invest 125, 1419–1432. 10.1172/JCI77993. [PubMed: 25705885]
60. Hunter WM, and Greenwood FC (1962). Preparation of iodine-131 labelled human growth hormone of high specific activity. Nature 194, 495–496. 10.1038/194495a0. [PubMed: 14450081]
61. Goetz DJ, Greif DM, Shen J, and Luscinskas FW (1999). Cell-cell adhesive interactions in an in vitro flow chamber. Methods Mol. Biol 96, 137–145. 10.1385/1-59259-258-9:137. [PubMed: 10098131]

Highlights

- Kindlin-3 is partially involved in attachment to high-density ICAM1 and HEV
- Co-occupancy of LFA1 with ICAM1 and talin1 activates Rap1 and induces slow rolling
- Distinct Rap1 impacts on affinity of integrins with different outcomes under flow

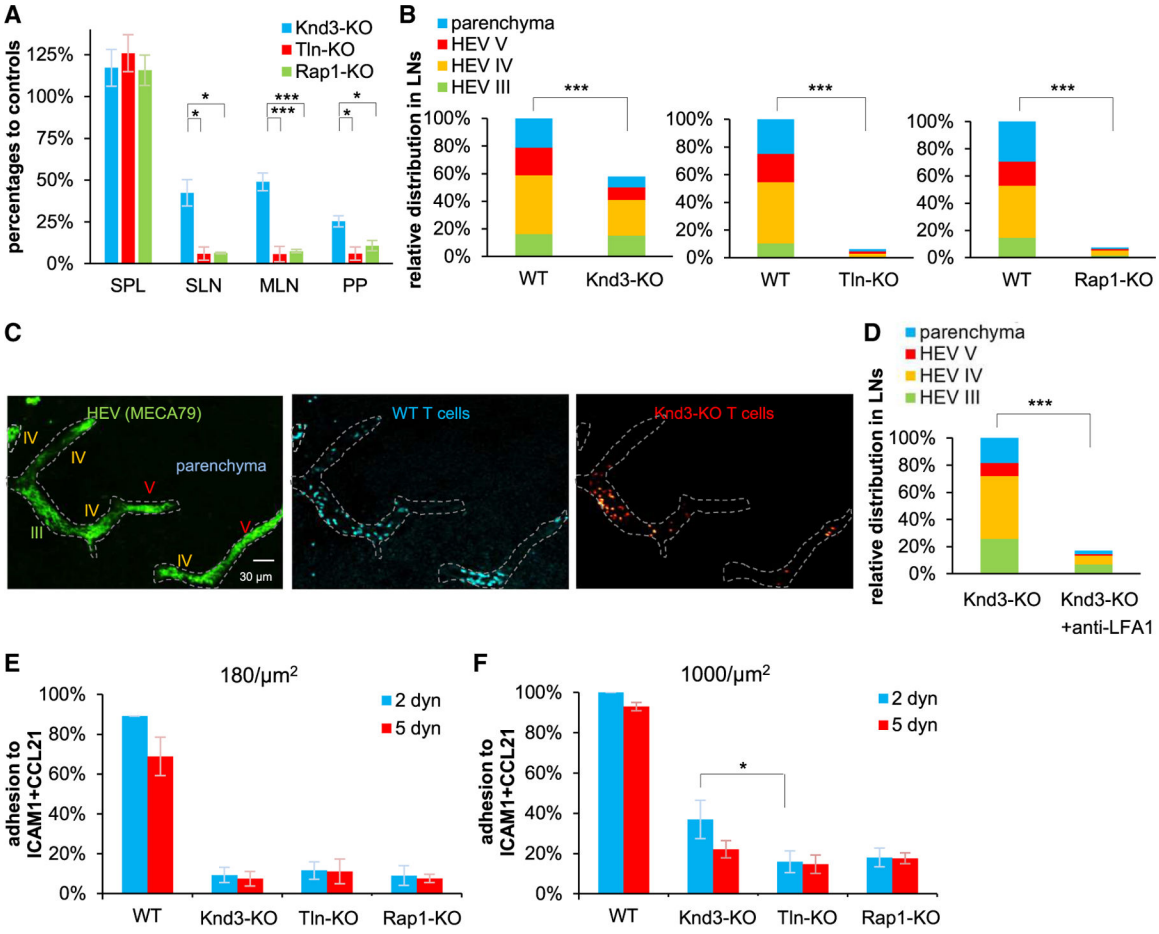

Figure 1. Requirement of Rap1, talin1, and kindlin-3 in lymphocyte homing

(A) *In vivo* short homing assay with fluorescently labeled T cells from kindlin-3-deficient (Knd3-KO), talin1-deficient (Tln-KO), or Rap1a/b double-deficient (Rap1-KO) mice. Labeled T cells harvested from spleen (SPL), surface LN (SLN), mesenteric LN (MLN), and Peyer's patches (PPs) were analyzed. The ratio against control T cells in tissues was calculated as homing efficiency. All experiments were performed in quadruplicate and statistically analyzed by Student's t test. Data are mean ± SD. Total analyzed cell numbers are 96,883 cells (SPL), 24,600 cells (SLN), 25,771 cells (MLN), and 10,949 cells (PP). (B) Relative distributions of transferred Knd3-KO, Tln-KO, or Rap1-KO T cells in LNs. HEVs III, >30 μm (diameter); HEVs IV, 20–30 μm with branches; HEVs V, < 20 μm; and parenchyma (outside of vessels). For the control experiment, dyes were swapped. All experiments were performed in duplicate at minimum and statistically analyzed by chi-squared test. Total counted cell numbers were 2,667 for WT, 1,384 for Knd3-KO (left), 4,071 for WT, 397 for Tln-KO (center), 1,984 for WT, and 163 for Rap1-KO T cells (right). (C) Representative images of transferred T cell distribution in LN slices. Transferred WT T cells (blue) were distributed in HEV orders III, IV, V (green), and parenchyma. Knd3-KO T cells (red) were sparsely distributed, especially in narrow HEVs (order IV and V) and parenchyma. Bar, 30 μm.

(D) Residual Knd3-KO T cells in HEVs were reduced by treatment with integrin-blocking Ab against integrin αL. Experiments were performed in duplicate and statistically analyzed by chi-squared test. Total cell numbers were 617 for Knd3-KO and 105 for Knd3-KO T cells with antibody blocking.

(E) Detachment assay of WT, Knd3-KO, Tln-KO, or Rap1-KO T cells on 180 sites/μm^2 of ICAM1 at 2 and 5 dyn/cm^2. Total numbers of input cells were 1,138 for the Knd3-KO control, 994 for Knd3-KO, 902 for the Tln-KO control, 721 for Tln-KO, 676 for the Rap1-KO control, and 805 for Rap1-KO T cells. All experiments were performed in triplicate at minimum and statistically analyzed by Student's t test.

(F) Detachment assay of WT, Knd3-KO, Tln-KO, or Rap1-KO T cells on 1,000 sites/μm^2 of ICAM1 at 2 and 5 dyn/cm^2. The total numbers of input cells were 2,282 for the control, 1,754 for Knd3-KO, 2,236 for Tln-KO, and 2,060 for Rap1-KO T cells. All experiments were performed in quadruplicate and statistically analyzed by Student's t test. Data are mean ± SD.

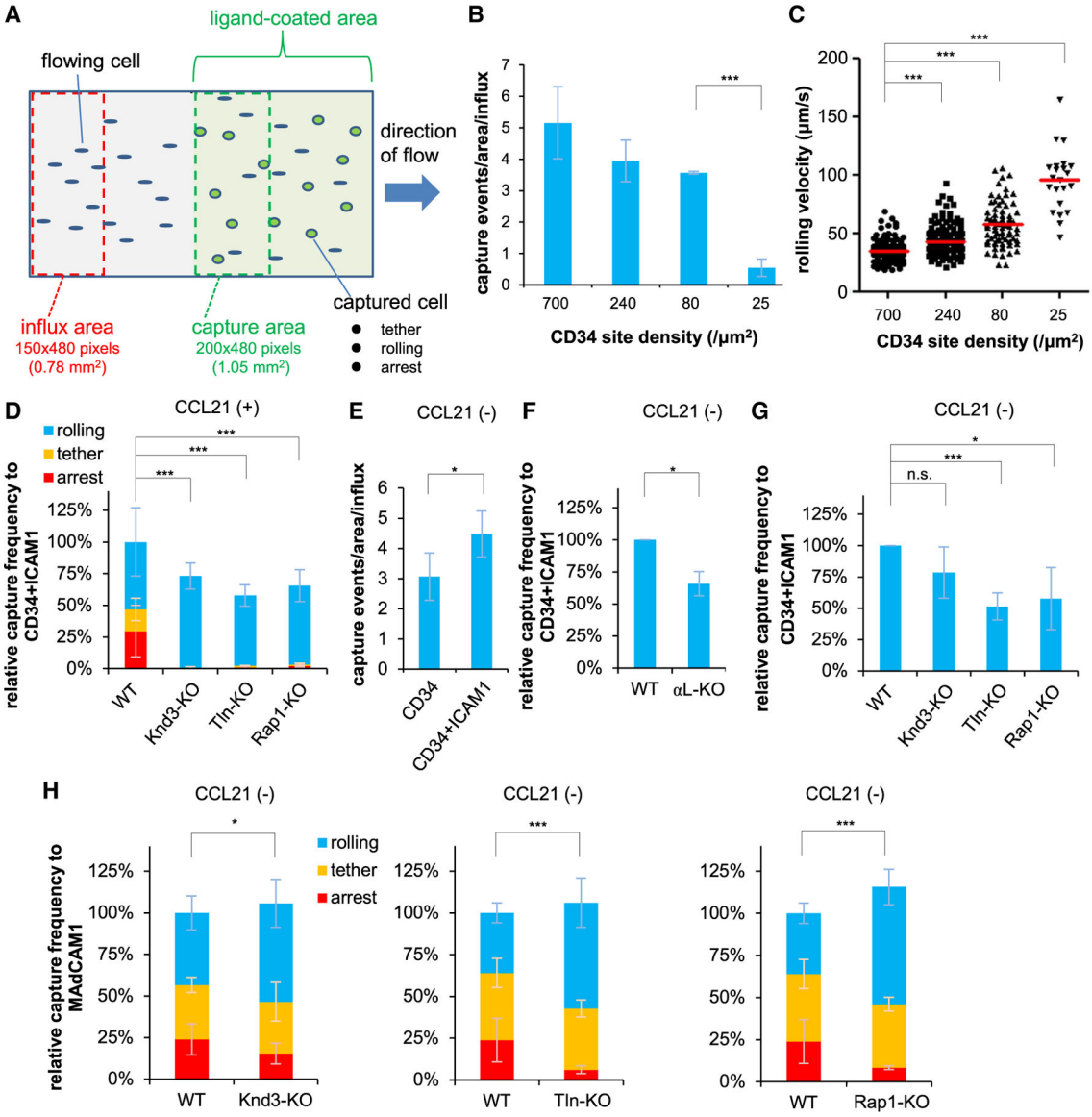

Figure 2. LFA1-ICAM1 interactions increase L-selectin-mediated tether/rolling

(A) A schematic cartoon of the flow experiment. The upstream part of a flow chamber was masked by a silicon rubber for measurement of cell influx in the flow. T cells were loaded in the glass syringe and infused into the flow chamber at the shear stress indicated. After shear flow was stable, bright-field images (640 × 480 pixels) were acquired at 30 frames/s (fps). Captured images were background subtracted and split into the influx area (non-coated area) and the capture area (ligand-coated area). Cell influx was determined by cell numbers in each frame and normalized for time and area (cell numbers/s/mm^2).

(B)Capture (rolling) events on PNAd$^+$CD34 (700 sites/μm^2, 240 sites/μm^2, 80 sites/μm^2, and 25 sites/μm^2) of WT T cells (267 cells, 242 cells, 177 cells, and 28 cells, respectively) were normalized by area (capture area) and influx at a flow rate of 3 dyn/cm^2. All experiments were performed in duplicate and statistically analyzed by Student's t test. Data are mean ± SD.

(C)Rolling velocities from individual cell trajectories were plotted at 25–700 sites/μm^2 of PNAd$^+$CD34 in (B) at a flow rate of 3 dyn/cm^2. Bars (red) indicate average. All experiments were performed in duplicate and statistically analyzed by Student's t test.

(D) Relative capture frequencies on PNAd$^+$CD34 (240 sites/μm^2) and ICAM1 (100 sites/μm^2) at a flow rate of 3 dyn/cm^2 with CCL21. Capture events/area of Knd3-KO (124 cells), Tln-KO (116 cells), or Rap1-KO T cells (145 cells) were normalized to that of WT (160 cells) and influx. All experiments were performed in triplicate and statistically analyzed by chi-squared test. Data are mean ± SD.

(E) Capture (rolling) events of WT T cells on PNAd$^+$CD34 (240 sites/μm^2) with or without ICAM1 (100 sites/μm^2) at a flow rate of 3 dyn/cm^2 without CCL21; 187 cells (on PNAd$^+$CD34) and 227 cells (on PNAd$^+$CD34 and ICAM1) were analyzed by Student's t test in triplicate. Data are mean ± SD.

(F) Relative capture (rolling) frequencies of αL-KO cells on PNAd$^+$CD34 (120 sites/μm^2) and ICAM1 (100 sites/μm^2) at a flow rate of 3 dyn/cm^2 without CCL21. WT (283 cells) and αL-KO T cells (202 cells) were analyzed by Student's t test in quadruplicate. Data are mean ± SD.

(G) Relative capture (rolling) frequencies of WT (535 cells), Knd3-KO (431 cells), Tln-KO (326 cells), or Rap1-KO T cells (323 cells) on PNAd$^+$CD34 (240 sites/μm^2) and ICAM1 (100 sites/μm^2) at a flow rate of 3 dyn/cm^2 without CCL21. All experiments were performed in quadruplicate and statistically analyzed by Student's t test. Data are mean ± SD.

(H) Relative capture frequencies of WT (274 cells for the Knd3KO control, 320 cells each for the Tln-KO control and Rap1-KO), Knd3-KO (220 cells), Tln-KO (255 cells), or Rap1-KO (279 cells) naive T cells on MAdCAM1 (270 sites/μm^2) at a flow rate of 3 dyn/cm^2. All experiments were performed in quadruplicate and statistically analyzed by chi-squared test. Data are mean ± SD.

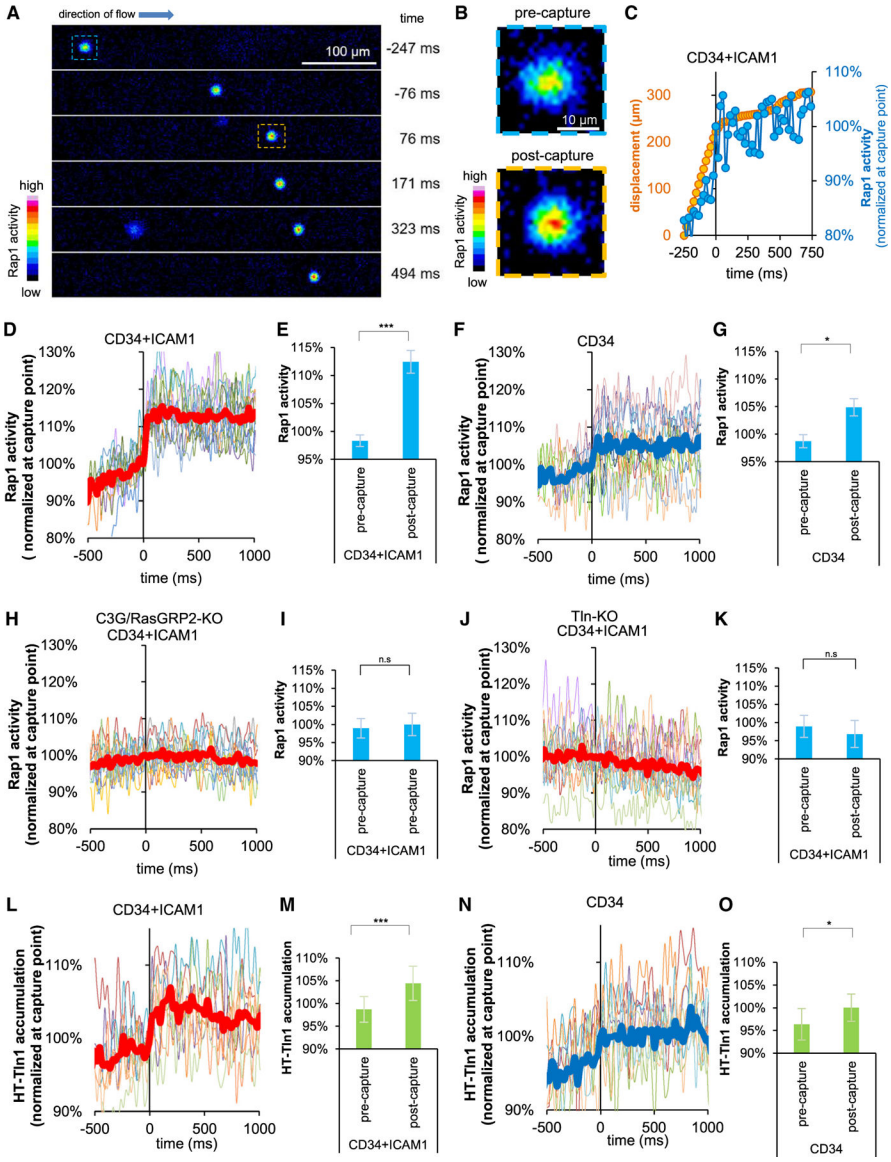

Figure 3. Increased Rap1 activation in rolling T cells by LFA1-ICAM1 interactions

(A) Rap1 activity was measured in a cultured T cell expressing GFP-RalGDS on PNAd^{+}CD34 (120 sites/μm^{2}) and ICAM1 (100 sites/μm^{2}) at a flow rate of 2 dyn/cm^{2}. Bar, 100 μm. The zero time point was set at a turning point where rolling velocity started to decelerate (capture).

(B) Magnified images of the pre-capture (blue dotted rectangle) and post-capture (orange dotted rectangle) events shown in (A). Bar, 10 μm.

(C) Time course of Rap1 activity (blue) and displacement (orange) in (A). Plot of intensities of the Rap1 affinity probe with the displacement curve of the rolling T cell indicated that increased intensities occurred concurrently with capture. Rap1 activity was normalized at time zero.

(D) Rap1 activity from individual cultured T cells (n = 14) and the average (thick red) on PNAd^{+}CD34 (120 sites/μm^{2}) and ICAM1 (100 sites/μm^{2}) at a flow rate of 2 dyn/cm^{2}.

(E) Statistical analysis of Rap1 activities of pre- and post-capture events in (D) by Student's t test. Pre-capture and post-capture events were determined from average intensities in 10 frames (0.2 s) before the capture and 10 frames after the capture, respectively.
(F) Rap1 activity from individually cultured T cells (n = 14) and the average (thick blue) on $PNAd^{+}CD34$ (120 sites/μm^2) at a flow rate of 2 dyn/cm^2.
(G) Statistical analysis of Rap1 activities of pre- and post-capture events in (F) by Student's t test.
(H) Rap1 activity from individually cultured C3G/RasGRP2-KO T cells (n = 14) and the average (thick red) on $PNAd^{+}CD34$ (120 sites/μm^2) and ICAM1 (100 sites/μm^2) at a flow rate of 2 dyn/cm^2.
(I) Statistical analysis of Rap1 activities of pre- and post-capture events in (H) by Student's t test.
(J) Rap1 activity from individual cultured Tln-KO T cells (n = 14) and the average (thick red) on $PNAd^{+}CD34$ (120 sites/μm^2) and ICAM1 (100 sites/μm^2) at a flow rate of 2 dyn/cm^2.
(K) Statistical analysis of Rap1 activities of pre- and post-capture events in (J) by Student's t test.
(L) Accumulation of talin1 from individual T cells (n = 12) and the average on $PNAd^{+}CD34$ (120 sites/μm^2) and ICAM1 (100 sites/μm^2) at a flow rate of 2 dyn/cm^2.
(M) Statistical analysis of talin1 accumulation of pre- and post-capture events in (L) was performed by Student's t test, as in (E).
(N) Accumulation of talin1 from individual T cells (n = 12) and the average on $PNAd^{+}CD34$ (120 sites/μm^2).
(O) Statistical analysis of talin1 accumulation of pre- and post-capture events in (N) by Student's t test.

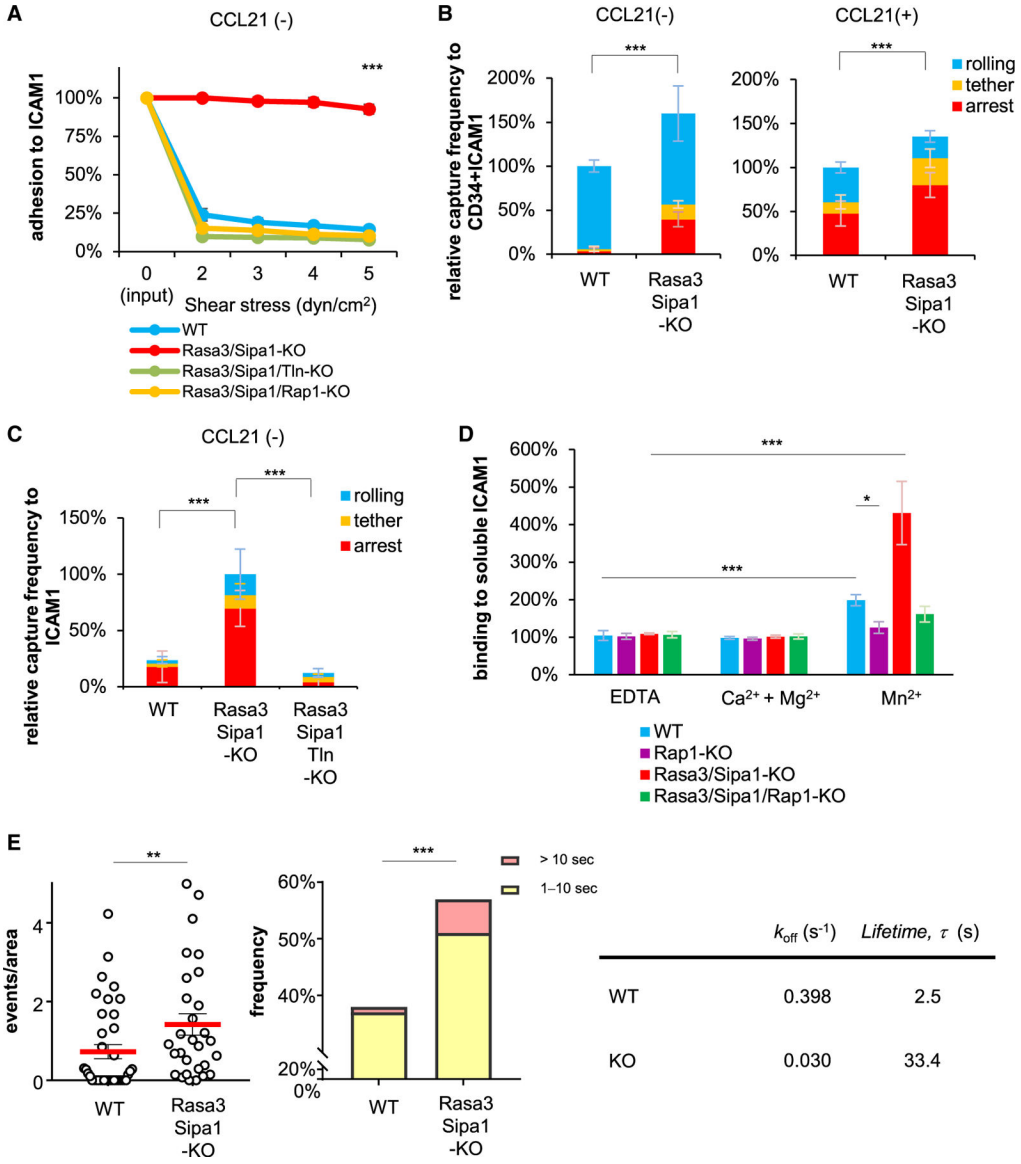

	k_{off} (s^{-1})	*Lifetime*, τ (s)
WT	0.398	2.5
KO	0.030	33.4

Figure 4. Impacts of RapGAP deficiencies in T cells on adhesion to ICAM1 in static and flow conditions

(A) Detachment assays with WT, Rasa3/Sipa1 double-deficient (Rasa3/Sipa1-KO), Rasa3/Sipa1/Talin1 triple-deficient (Rasa3/Sipa1/Tln-KO), or Rasa3/Sipa1/Rap1a/Rap1b quadruple-deficient (Rasa3/Sipa1/Rap1a/Rap1b-KO) T cells on ICAM1 (180 sites/μm^2) without CCL21 at a flow rate of 2–5 dyn/cm^2. Total numbers of input cells were 1,163 for the control, 762 for Rasa3/Sipa1-KO, 946 for Rasa3/Sipa1/Tln-KO, and 955 for Rasa3/Sipa1/Rap1a/Rap1b-KO T cells. All experiments were performed in triplicate and statistically analyzed by Student's t test (Rasa3/Sipa1-KO and WT at 5 dyn/cm^2). Data are mean ± SD.

(B) Relative capture frequencies of WT (239 cells) or Rasa3/Sipa1-KO T cells (300 cells) on $PNAd^+CD34$ (120 sites/μm^2) and ICAM1 (100 sites/μm^2) without CCL21 (left) under 2 dyn/cm^2 flow. Relative capture frequencies of WT (88 cells) or Rasa3/Sipa1-KO T cells (115 cells) on $PNAd^+CD34$ and ICAM1 with CCL21 (right) at a flow rate of 2 dyn/cm^2.

All experiments were performed in duplicate at minimum and statistically analyzed by chi-squared test. Data are mean ± SD.

(C) Relative capture frequency of WT (20 cells), Rasa3/Sipa1-KO (79 cells), or Rasa3/Sipa1/Tln-KO T cells (9 cells) on ICAM1 (100 sites/μm^2) without CCL21 at a flow rate of 2 dyn/cm^2. All experiments were performed in triplicate and statistically analyzed by chi-squared t test. Data are mean ± SD.

(D) Binding assays to soluble ICAM1 of WT and mutant T cells were performed in the presence of EDTA (5 mM), Ca^{2+} (0.5 mM) and Mg^{2+} (0.5 mM), and Mn^{2+} (1 mM). Data are mean ± SD for the three independent experiments.

(E) Single-molecule analysis of LFA1-ICAM1 interaction of WT or Rasa3/Sipa1-KO T cells in the presence of Ca^{2+} and Mg^{2+} (0.5 mM each). The site density of ICAM1 was 300 molecules/μm^2. Data are mean ± SD. (Left) Frequencies of LFA1-ICAM1 interaction events normalized by adhesion area. Each circle indicates events per area from a single cell. n = 38 (WT) and n = 29 (Rasa3/Sipa1-KO). Statistical significance was calculated by Student's t test. (Middle) Histogram of frequencies of LFA1-ICAM1 binding events with lifetimes from 1 to 10 s (yellow) or longer than 10 s (pink) of WT (n = 138) and Rasa3/Sipa1-KO (n = 309) T cells. Statistical significance was calculated by chi-squared t test. (Right) The dissociation rate constants (k_{off}, s^{-1}) and average lifetime (τ, s) of LFA1-ICAM1 interaction on WT and Rasa3/Sipa1-KO T cells.

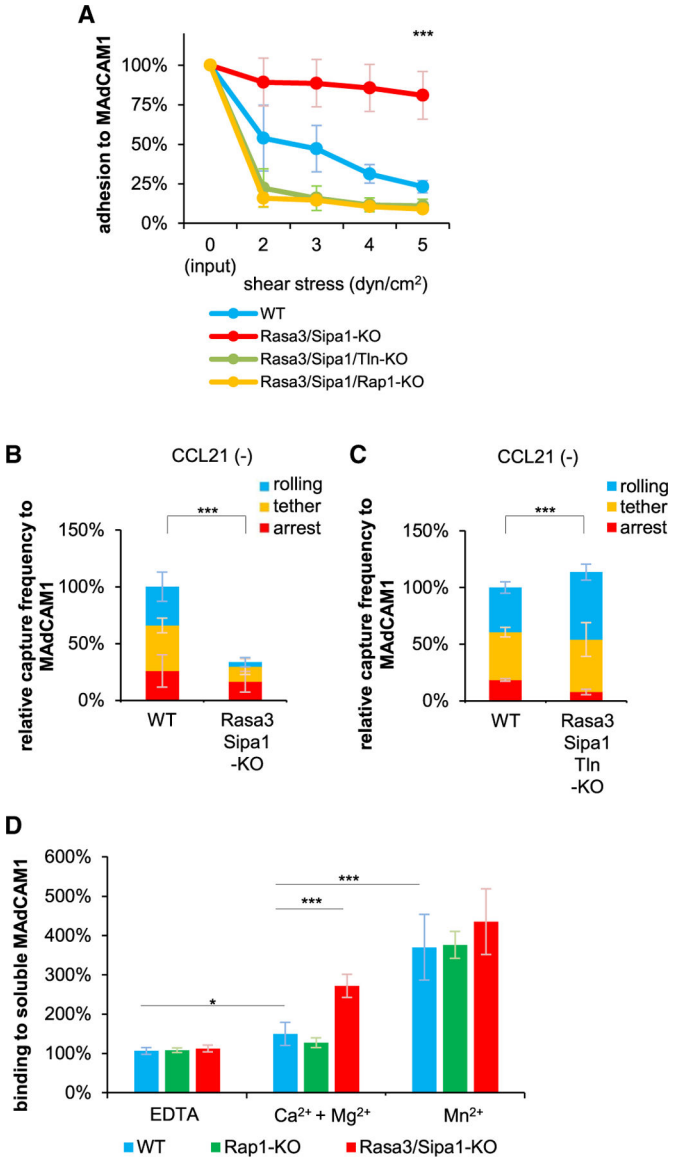

Figure 5. High-affinity α4β7 induced by activated Rap1 inhibits adhesion to MAdCAM1 under flow

(A) Detachment assays with WT, Rasa3/Sipa1-KO, Rasa3/Sipa1/Tln-KO, or Rasa3/Sipa1/Rap1a/Rap1b-KO T cells on MAdCAM1 (270 sites/μm^2) without CCL21 at a flow rate of 2–5 dyn/cm^2. Total numbers of input cells were 1,326 for the control (WT), 1,047 for Rasa3/Sipa1-KO, 890 for Rasa3/Sipa1/Tln-KO, and 949 for Rasa3/Sipa1/Rap1a/Rap1b-KO T cells. All experiments were performed in triplicate and statistically analyzed by Student's t test (Rasa3/Sipa1-KO and WT at 5 dyn/cm^2). Data are mean ± SD.

(B and C) Relative capture frequency of WT (270 cells for the Rasa3/Sipa1-KO control and 203 cells for the Rasa3/Sipa1/Tln-KO control), Rasa3/Sipa1-KO (62 cells), or Rasa3/Sipa1/Tln-KO T cells (130 cells) on MAdCAM1 without CCL21 at a flow rate of 3 dyn/cm^2. All experiments were performed at least in triplicate at minimum and statistically analyzed by chi-squared t test. Data are mean ± SD.

(D) Binding assays to soluble MAdCAM1 of WT and mutant T cells were performed in the presence of EDTA (5 mM), Ca^{2+} and Mg^{2+} (0.5 mM each), and Mn^{2+} (1 mM). Data are mean ± SD of three independent experiments.

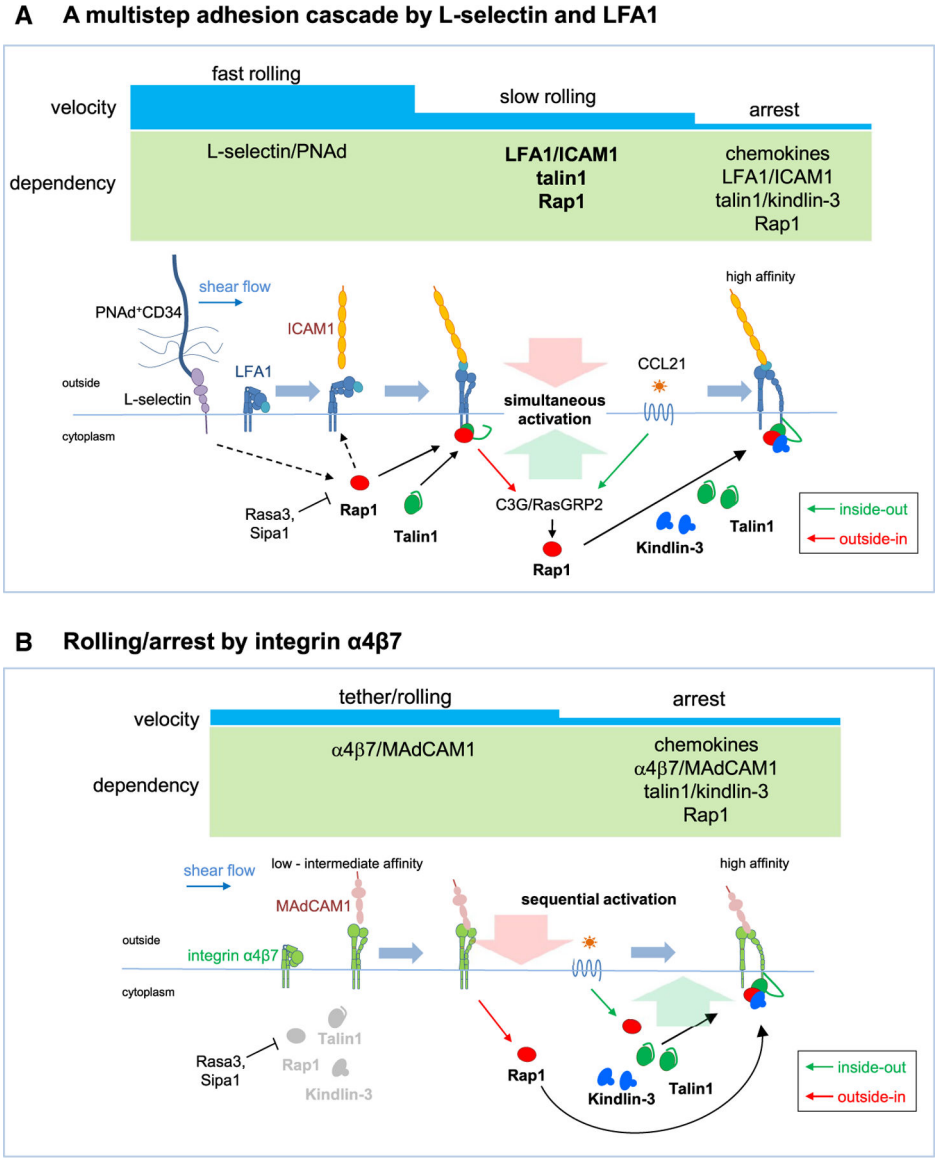

Figure 6. Models of bidirectional regulation of LFA1 and α4β7 in T cells

(A) A multistep adhesion cascade by L-selectin and LFA1. L-selectin interacting with PNAd$^+$ CD34 mediates a capture and initiates tether/fast rolling with a minimal level of activated Rap1 and talin1 recruitment. Simultaneous occupancy of LFA1 with ICAM1 and talin1 results in conformational changes of LFA1 from bent/low affinity to extended/intermediate affinity and transmits the outside-in signaling through subsecond activation of Rap1, which recruits talin1, increasing the capture and decreasing rolling velocities (slow rolling). A further increase of Rap1 activation by CCL21 results in more recruitment of talin1, leading to talin1/kindlin-3-dependent arrest by high-affinity bindings of LFA1 to ICAM1. Rap1 activation and inactivation occurs via RasGRP2/C3G and Rasa3/Sipa1, respectively.

(B) Rolling and arrest by α4β7. Interactions with α4β7 with MAdCAM1 support tether/rolling in a manner independent of Rap1, talin1, and kindlin-3, all of which require

subsequent chemokine-induced arrest. Ligand-induced arrest without chemokines also occurs in a lesser degree, which requires Rap1 and talin1 with a marginal contribution of kindlin-3. High basal levels of activated Rap1 due to the loss of Rasa3/Sipa1 generates high-affinity α4β7, which results in inhibition of adhesive interactions under flow (see text). Sequential activation processes by outside-in and inside-out signaling induce efficient rolling and arrest by α4β7.

KEY RESOURCES TABLE

REAGENT or RESOURCE	SOURCE	IDENTIFIER
Antibodies		
Alexa Fluor 647 Rat anti-mouse/human PNAd	Biolegend	Cat# 120808; RRID: AB_2783060
Alexa Fluor 594 Rat anti-mouse/human PNAd	Biolegend	Cat# 120805; RRID: AB_2650843
Alexa Fluor 488 Rat anti-mouse/human PNAd	Thermo Fisher Scientific	Cat# 53–6036-80; RRID:AB_10804391
APC Armenian Hamster anti-mouse CD3ϵ	Biolegend	Cat# 100312; RRID: AB_312677
APC Rat anti-mouse CD4	Biolegend	Cat# 100411; RRID: AB_312696
APC Rat anti-mouse CD8a	Biolegend	Cat# 100712; RRID: AB_312751
Biotin Rat anti-mouse CD45	Biolegend	Cat# 103103; RRID: AB_312968
Biotin Rat anti-mouse/human CD45R/B220	Biolegend	Cat# 103204; RRID: AB_312989
Biotin Rat anti-mouse/human CD44	Biolegend	Cat# 103004; RRID: AB_312955
Biotin Rat anti-mouse F4/80	Biolegend	Cat# 123105; RRID: AB_893499
Biotin Rat anti-mouse CD11a	Biolegend	Cat# 101103; RRID: AB_312776
Biotin Rat anti-mouse CD11b	Biolegend	Cat# 101204; RRID: AB_312787
Biotin Rat anti-mouse CD11c	Biolegend	Cat# 117304; RRID: AB_313773
Biotin Rat anti-mouse CD4	Biolegend	Cat# 100507; RRID: AB_312710
Biotin Rat anti-mouse CD8a	Biolegend	Cat# 100703; RRID: AB_312742
Biotin Rat anti-mouse TER-119	Biolegend	Cat# 116203; RRID: AB_313704
Biotin Rat anti-mouse Ly-6G/Ly-6C	Thermo Fisher Scientific	Cat# 13–5931-82; RRID: AB_466800
CD45R (B220) Monoclonal Antibody (RA3–6B2), eFluor 450	Thermo Fisher Scientific	Cat# 48–0452-82; RRID:AB_1548761
FITC Rat anti-mouse CD62L	Biolegend	Cat# 104406; RRID: AB_313093
FITC Rat anti-mouse CD11a	Biolegend	Cat# 101106; RRID: AB_312779
FITC Rat anti-mouse CD34	Thermo Fisher Scientific	Cat# 11–0341-81; RRID: AB_465021
FITC Rat anti-mouse CD44	Biolegend	Cat# 103006; RRID: AB_312957
PE Rat anti-mouse/human CD44	Biolegend	Cat# 103008; RRID: AB_312959
PE Rat anti-mouse LPAM-1 (Integrin α4β7)	Biolegend	Cat# 120605; RRID: AB_493268
PE Rat anti-mouse CD62L	Biolegend	Cat# 104407; RRID: AB_313094
PE Rat anti-mouse CD11a	Biolegend	Cat# 12–0111-81; RRID: AB_465544
Purified anti-mouse/human PNAd	Biolegend	Cat# 120802; RRID: AB_493555
Purified anti-mouse CD54 (ICAM-1)	Biolegend	Cat# 116101; RRID: AB_313692
Purified anti-mouse CD28	Biolegend	Cat# 102116; RRID: AB_11147170
Purified anti-mouse CD3ϵ	Biolegend	Cat# 100340; RRID: AB_11149115
Purified anti-mouse MAdCAM-1 (MECA-89) from hybridoma	ATCC/This paper	Cat# HB-292
Purified anti-mouse CD62L (MEL-14) from hybridoma	ATCC/This paper	Cat# HB-132
Purified anti-mouse ICAM-1 from hybridoma	ATCC/This paper	Cat# CRL-1878
Purified anti-mouse CD11a (KBA) from hybridoma	Kondo et al.[22]	N/A
Rabbit anti-human IgG F(c) Antibody	Rockland	Cat# 609–4103
Aelxa488 Goat anti-human IgG	Thermo Fisher Scientific	Cat# A-11013
Kindlin1 Polyclonal antibody	Proteintech	Cat# 22215–1-AP
Kindlin2 Polyclonal antibody	Proteintech	Cat# 11453–1-AP

REAGENT or RESOURCE	SOURCE	IDENTIFIER
Anti-URP2/Kindlin-3 antibody	Abcam	Cat# ab68040
Talin1/2 Monoclonal antibody (8d4)	Sigma	Cat# T3287
Monoclonal Anti-α-Tubulin antibody (DM1A)	Sigma	Cat# T9026
Anti CD34 (TUK3)	Santa Cruz Biotechnology	Cat# sc-19587
Monoclonal anti-Rap1	BD Biosciences	Cat# 610196; RRID: AB_397595
RASGRP2 Polyclonal Antibody	Thermo Fisher Scientific	Cat# PA5–28865; RRID: AB_2546341
Anti-Rasgrp1 (C3G) antibody	Abcam	Cat# ab37927
Anti-rabbit IgG, HRP-linked Antibody	Cell Signaling Technology	Cat# 7074; RRID: AB_2099233
Anti-mouse IgG, HRP-linked Antibody	Cell Signaling Technology	Cat# 7076; RRID: AB_330924
Chemicals, peptides, and recombinant proteins		
CellTrace CFSE Cell Proliferation Kit	Thermo Fisher Scientific	Cat# C34554
CellTracker Blue CMF_2HC Dye	Thermo Fisher Scientific	Cat# C12881
CellTracker Orange CMTMR Dye	Thermo Fisher Scientific	Cat# C2927
Recombinant Mouse ICAM-1 Fc Chimera	Ueda et al.[25]	N/A
Recombinant Human $PNAd^+$ CD34 Fc Chimera	This paper	N/A
Recombinant Mouse MAdCAM-1 Fc Chimera	R&D	Cat# 993-MC-050
Recombinant Rat $PNAd^+$ MAdCAM-1 Fc Chimera	This paper	N/A
Western Lightning Plus-ECL	PerkinElmer	Cat# NEL 104001EA
Recombinant human IL-2	Peprotech	Cat# 200–02
Recombinant Mouse CCL21/6Ckine Protein	R&D	Cat# 457–6C-025/CF
PMA	Sigma	Cat# P1585–1MG
Lympholyte M	Cedarlane Laboratories	Cat# CL5031
IMDM medium	Thermo Fisher Scientific	Cat# 12440–061
Carrier-free $Na^{125}I$	PerkinElmer	Cat# NEZ033A
Chloramine T Trihydrate	Tokyo Chemical Industry	Cat# C0076
Sodium Iodide	Tokyo Chemical Industry	Cat# S0564
Sodium metabisulfite	Sigma	Cat# 161519
GST-RalGDS-RBD	Ueda et al.[25]	N/A
7-AAD Viability Staining Solution	Biolegend	Cat# 420404
ATTO647N-NHS-ester	ATTO-TEC	Cat# AD647N-31
1,2-dioleoyl-sn-glycero-3-phosphoethanolamine-N-(cap biotinyl) (sodium salt)	Avanti Polar Lipids	Cat# 870273C
1,2-dioleoyl-sn-glycero-3-phosphocholine	Avanti Polar Lipids	Cat# 850375C
SaraFluor650T ligand	Goryo chemical	Cat# A308–02
Critical commercial assays		
Mojosort Mouse CD3 T cell Isolation Kit	Biolegend	Cat# 480031
Experimental models: Cell lines		
Mouse Primary T cells	This paper	N/A
Human 293T cell	ATCC	CRL-3216

REAGENT or RESOURCE	SOURCE	IDENTIFIER
Human LS12 cell	Kimura et al.[44]	N/A
Experimental models: Organisms/strains		
Mouse: C57BL/6	CLEA Japan	Ordering name: C57BL/6JJcl
Mouse: B6.Cg-Tg(CD4-cre)1Cwi N9	Taconic	Stock No: 4196
Mouse: B6.Rap1a$^{f/f}$; Rap1b$^{f/f}$	Ueda et al.[25]	N/A
Mouse: B6.129P2-Tln1$^{tm4.1Crit}$	The National Mouse Archive	Strain ID: EM:04999
ES: Fermt3$^{tm1a(KOMP)Wtsi}$	KOMP	MMRRC:055592-UCD
Mouse: B6.C3G$^{f/f}$	This paper	N/A
Mouse: B6.RasGRP2$^{f/f}$	This paper	N/A
Mouse: B6.Rasa3$^{f/f}$	Stefanini et al.[30]	N/A
Mouse: B6.Itgal$^{-/-}$	Schmits et al.[56]	N/A
Mouse: B6.Sipa1$^{-/-}$	Ueda et al. under review	N/A
Mouse: B6.HT-Tln1$^{KI/KI}$	This paper	N/A
Recombinant DNA		
CSII EF MCS/Ral GDS GFP (GFP-fused RalGDS-RBD)	Ueda et al.[25]	N/A
CSII EF Venus	This paper	N/A
pCAG-HIVgp	Riken BRC	RDB04394
pCMV-VSV-G-RSV-Rev	Riken BRC	RDB04393
pIG vector	Katagiri et al.[57]	N/A
Fuc-T VII cDNA	Kimura et al.[44]	N/A
6-Sul-T cDNA	Kimura et al.[44]	N/A
Software and algorithms		
MATLAB	Mathworks	https://www.mathworks.com/products/matlab
Prism 5	GraphPad Software Inc.	https://www.graphpad.com
Metamorph	Molecular Devices	https://www.moleculardevices.com/
Fiji	(open source)	https://imagej.net/
CellQuest	BD Biosciences	N/A
FlowJo v10	BD Biosciences	N/A
G-count and G-track software	G-angstrom, Japan	N/A
Excel	Microsoft	N/A
Other		
FCS2 Chamber	Bioptechs	https://bioptechs.com/
Polystyrene disks for FCS2 Chamber	This paper	NA
programmed syringe pump	MELQUEST, Japan	FP-1000
Vibratome	D.S.K, Japan	LinearSlicer Pro10
Disposable PD-10 Desalting Column with Sephadex G-25 resin	Cytiva	Cat# 17085101
35 mm glass bottom dish	Matsunami glass, Japan	Cat# D11130H

REAGENT or RESOURCE	SOURCE	IDENTIFIER
Protein G Sepharose 4 Fast Flow	Cytiva	Cat# 17061801
Glutathione Sepharose 4B	Cytiva	Cat# 17075601